DOI:
10.1109/TNB.2017.2669309

Document Version
Peer reviewed version

Modeling Contrast-imaging-assisted Optimal Targeted Drug Delivery: A Touchable Communication Channel Estimation and Waveform Design Perspective

Journal:	*Transactions on NanoBioscience*
Manuscript ID	TNB-00174-2016.R1
Manuscript Type:	Regular
Date Submitted by the Author:	n/a
Complete List of Authors:	Chen, Yifan; Southern University of Science and Technology Zhou, Yu; Southern University of Science and Technology; Hong Kong University of Science and Technology Murch, Ross; Hong Kong University of Science and Technology Kosmas, Panagiotis; King's College London, Informatics
Keywords:	Targeted drug delivery, Contrast-enhanced microwave imaging, Optimal targeted therapies, Touchable communication channel estimation and waveform design, Molecular communication

Modeling Contrast-imaging-assisted Optimal Targeted Drug Delivery: A Touchable Communication Channel Estimation and Waveform Design Perspective

Yifan Chen, Yu Zhou, Ross Murch, and Panagiotis Kosmas

Abstract

To maximize the effect of treatment and minimize adverse effects on patients, we propose to optimize nanorobots-assisted targeted drug delivery (TDD) for locoregional treatment of tumor from the perspective of touchable communication channel estimation and waveform design. The drug particles are information molecules; the loading/injection and unloading of the drug correspond to the transmitting and receiving processes; the concentration-time profile of drug particles administered corresponds to the signalling pulse. Given this analogy, we first propose to use contrast-enhanced microwave imaging (CMI) as a pretherapeutic evaluation technique to determine the pharmacokinetic model of nanorobots-assisted TDD. The CMI system applies an information-theoretic-criteria-based algorithm to estimate drug accumulation in tumor, which is analogous to the estimation of channel impulse response in the communication context. Subsequently, we present three strategies for optimal targeted therapies from the communication waveform design perspective, which are based on minimization of residual drug molecules at the end of each therapeutic session (i.e., inter-symbol interference), maximization of duration when the drug intensity is above a prespecified threshold during each therapeutic session (i.e., non-fade duration), and

Y. Chen is with the Faculty of Science and Engineering and the Faculty of Computing and Mathematical Sciences, the University of Waikato, Hamilton, New Zealand (e-mail: yifanc@waikato.ac.nz). He is also with the Department of Electrical and Electronic Engineering, Southern University of Science and Technology, Shenzhen, China (e-mail: chen.yf@sustc.edu.cn).

Y. Zhou is with the Department of Electrical and Electronic Engineering, Southern University of Science and Technology, Shenzhen, China. He is also with the Department of Electronic and Computer Engineering, Hong Kong University of Science and Technology, Hong Kong, China.

R. Murch is with the Department of Electronic and Computer Engineering, Hong Kong University of Science and Technology, Hong Kong, China.

P. Kosmas is with the Department of Informatics, King's College London, London, UK.

minimization of average rate that a therapeutic operation is not received correctly at tumor [i.e., bit error rate (BER)]. Finally, numerical examples are applied to demonstrate the effectiveness of the proposed analytical framework.

Index Terms

Targeted drug delivery, contrast-enhanced microwave imaging, optimal targeted therapies, touchable communication channel estimation and waveform design

I. Introduction

Nanoparticle-mediated targeted drug delivery (TDD) aims at enhancing locoregional therapies for cancer treatment [1]. These nanoparticles are loaded with drugs and targeted to specific parts of the body where there is solely diseased tissue, thereby avoiding interaction with healthy tissue. The main constraints of the nanocarriers currently administered are the reliance on systemic circulation resulting in only $\sim 2\%$ of the total administered dose being deposited in the tumor, the lack of a propelling force to penetrate the tumor beyond the diffusion limit, and the absence of a sensory-based displacement capability to target the hypoxic zones [2]. Harnessing swarms of magneto-aerotactic bacteria such as the *Magnetococcus marinus* strain MC-1 for delivering drug-containing nanoliposomes to the disease site can significantly improve the therapeutic index of various nanocarriers in tumor regions as demonstrated in [2]. It is crucial to obtain the appropriate concentration-time profile of the therapeutic agent to be injected with respect to the developmental stage of the tumor in order to maximize the effect of treatment and to minimize adverse effects on patients [3].

Molecular communication models can be applied to describe the TDD process [4]–[10]. In molecular communication, an engineered miniature transmitter emits molecules, which propagate and are eventually received by a miniature receiver. The information may be encoded in either the timing or the concentration of molecules. The reception process often involves a chemical reaction between molecules (ligand) and compliant receptors present on the receiver surface. Under this framework, the transmitting process for a TDD system is the drug injection, the receiving process is the drug delivery at a specific target (e.g., tumor), and the channel is realized by the transport of drug particles in the blood stream. The signal is the concentration-time profile of the therapeutic agent, which should be successfully received by the tumor to decrease its size.

This analogy enables the analysis and design of TDD using classical communication tools [4]–[10]. By applying the queuing theory to model receptor saturation, thus treating it as a congestion problem

in communication networks, the optimal drug release rate was estimated in [9] to guarantee that the desired fraction of receptors bound to drug molecules without drug overloading. By modeling the pharmacokinetics of TDD systems through the abstraction of molecular communication, including the particle advection, diffusion, absorption, reaction, and adhesion as well as the impact of cardiovascular diseases, the optimal drug injection rate was obtained in [7] to achieve a desired drug delivery rate. In [3], optimal control techniques were applied to find the appropriate treatment and drug dose to decrease the tumor size while minimizing total drug administered for antiangiogenic therapy, chemotherapy, and radiotherapy. Finally, optimal shape of the antibody molecular structure was determined in [6] by applying the antibody-mediated TDD system transport and antigen-binding kinetics, taking into account the geometry of the antibody molecule, the electrochemical structure of the antibody-antigen complex, and the physiology of the patient. Nevertheless, the existing works do not discuss how to obtain information of the vascular, extracellular, and ligand-binding channels, which is necessary in order to apply the proposed TDD strategies in real-life applications. Furthermore, none of the works has designed the drug concentration-time profile from the perspective of communication waveform optimization, where the transmission is organized in bursts of drug molecules (i.e., pulses denoting information bits).

The current contribution addresses the aforementioned problems by taking the following approaches. Firstly, interfaces to connect the small-scale *in vivo* environment and the large-scale external environment could be implemented under the paradigm of touchable communication as proposed in [8], [11]. The term "touchable" means that the entire communication process can be controlled and tracked *via* interfaces. Specifically, the in-messaging interfaces convert conventional electronic, magnetic, or optical signals used by the large-scale device into commands to which nanorobots respond by performing subsequent small-scale operations (e.g., through *magnetotaxis* directional control of MC-1 cells [2]), while the out-messaging interfaces convert motion signals generated by nanorobots (e.g., releasing, swimming, and targeting of nanorobots) to externally detectable and interpretable messages [12]. Contrast-enhanced microwave imaging (CMI) can be employed as the out-messaging interface, where the cargo attached to nanorobots is a microwave contrast agent such as carbon nanotubes, which can also serve as a therapeutic agent in cancer treatment [13], [14]. Hence, the CMI technique is proposed for estimation of the TDD pharmacokinetics (equivalently, the impulse response of the touchable communication channel), where two signal-to-noise-ratio (SNR) sensitive information-theoretic criteria [15] are applied to determine the drug disposition in tumor. This estimation step provides exact knowledge about the vascular channel specific to the individual patient and the TDD process undergone, thereby alleviating the issue of wide variety of vasculature across different patients.

Secondly, a novel signal transmission scheme suitable for TDD based on the estimated channel response and the on-off keying scheme is proposed. Three waveform design strategies are then suggested to achieve minimum inter-symbol interference, maximum non-fade duration, and minimum average bit error rate (BER). From the TDD perspective, these criteria yield low side-effects due to residual therapy damaging some healthy tissues after each therapeutic session, long duration when the concentration of drug molecules is sufficiently high, and low average rate that a therapeutic operation is not received correctly at tumor, respectively.

It is worth emphasizing that both the two contributions mentioned above, namely, the CMI for approximation of the TDD pharmacokinetics (channel estimation) and the optimal targeted therapies from the communication perspective (waveform design) have not been covered in our previous works [8], [11], which mainly focus on the general system architecture and channel modeling aspects.

The paper is organized as follows. In Section II, the system and channel models of touchable communication for optimal targeted therapies are investigated. In Section III, the CMI system for estimation of the channel impulse response is presented. In Section IV, the signal transmission process is studied and the waveform optimization strategies are introduced. Finally, Section V provides simulation studies of TDD to demonstrate the principles of the analytical framework, with conclusions drawn in Section VI.

II. Touchable Communication Model of Optimal TDD

The touchable communication model of TDD using drug-loaded nanorobots is illustrated in Fig. 1. The information molecules are therapeutic agents. The binding of drug particles to a swarm of nanorobots such as magneto-aerotactic bacteria and the injection of the swarm into the vascular network at a predefined site are the transmitting process. The transmitted signal $x_{\mathrm{T}}(t)$ is the amount of injected nanoparticles. An external macro-unit generates a magnetic field; the nanorobots sense this field and move towards its gradient *via* magnetotaxis. The propagation process is the touchable communication channel. When the nanorobots reach the tumor, the drug particles will be removed from the vehicles and get assimilated into the targeted issue allowing them to perform healing actions. The unloading operation corresponds to the receiving process. The received signal $x_{\mathrm{R}}(t)$ is the number of nanoparticles successfully discharged at the tumor.

A. Signal Transmission Model

The amount of administered therapeutic agent must be carefully chosen to destroy the tumor, while causing minimal injuries to healthy tissues due to leakage of drug molecules to the systemic flow. To

address this issue, optimal control theories have been applied for antiangiogenic therapy, chemotherapy, or radiotherapy [16], [17]. The adaptation of these conventional therapies to the case of magnetically controlled drug-loaded nanoparticles was presented in [3]. Given the specific tumor growth model (e.g., the classical Hahnfeldt's model [18] and its extension [3], [16]), the issue is to find an optimal control input u to decrease the tumor size while minimizing total drug administered. A maximum drug intake $u_{\max}$ has to be enforced. Furthermore, a continuous administration of therapeutic agent has to be realized [3].

From the communication perspective, the transmission process associated with the aforementioned drug administration can be arranged using an on-off scheme consisting of multiple time slots. The period of each slot is T_{slot} as illustrated in Fig. 1, which corresponds to the communication symbol duration. A bit '0' is denoted by the absence of molecule within a time slot. On the other hand, a bit '1' is denoted by a burst of molecules $x_{\text{T}}(t)$ over a short period equal to T_{burst} where $T_{\text{burst}} \leq T_{\text{slot}}$. For normalized $x_{\text{T}}(t)$ satisfying $\int_0^{T_{\text{slot}}} x_{\text{T}}(t)dt = \int_0^{T_{\text{burst}}} x_{\text{T}}(t)dt = 1$, the optimal control input u_i emulated by the i^{th} cluster of continuous emissions of drug molecules is:

$$\begin{aligned} u_i &= \int_0^{u_i T_{\text{slot}}} x_{\text{T}}(t)dt \\ &= u_i \int_0^{T_{\text{burst}}} x_{\text{T}}(t)dt. \end{aligned} \tag{1}$$

As such, u_i also denotes the number of bits over the i^{th} cluster of continuous emissions. Furthermore, the drug intake has to be saturated to an upper limit such that $u_i \leq u_{\max}$. This on-off scheme represents both a clinically relevant drug administration process and a useful analytical framework for optimal direct targeting therapy under the rubric of information transmission, which allows for application of the classical communication performance measures such as inter-symbol interference, non-fade duration, and BER to system design as to be made clear in the following sections.

B. Signal Reception Model

The signal reception process is characterized by the pharmacokinetics model, which describes how the therapeutic agent is absorbed, distributed, and eliminated by the body and is commonly modeled through the agent concentration in the sampled fluid (e.g., plasma or blood) at the host, $x_{\text{R}}(t)$. A compartmental modeling analysis has been widely employed. For example, the compartment models best-fit the concentration-time profiles of plasma temozolomide, which is an agent effective for treating gliomas, in cerebrospinal fluid, normal brain, and brain tumor tissues in a rat orthotopic brain tumor model [19]. The one-compartment model was applied in modeling the biodistribution of drug-loaded

magnetic nanoparticles for the liver cancer [3], which is similar to the situation of nanorobots-assisted TDD considered here. Under this circumstance, the input is equal to the dose at the initial time point 0 and becomes 0 thereafter. The concentration at time 0 corresponds to the dose divided by the volume of the tumor, and the concentration decreases with time in an exponential manner.

Hence, the following agent concentration expression is derived:

$$x_{\mathrm{R}}(t) = \int_{\tau} \rho x_{\mathrm{T}}(\tau) \exp\left[-\zeta(t-\tau)\right] d\tau, \tag{2}$$

where ρ is the path loss from the injection site to the tumor and ζ is the drug clearance rate. The path loss consists of three different components for touchable communication [8]: diffusion, branching, and resorption. Each loss component reduces certain amount of nanorobots, and the overall attenuation is obtained as the multiplication of these components. The diffusion occurs in the systemic flow due to the random Brownian motions of nanorobots; the branching occurs at the entrance of the intended daughter branch when the vessels are too slender to be imaged. The resorption quantifies the effect of biodegradation on the amount of nanorobots consumed. Detailed derivations of the path loss ρ can be found in [8]. As ρ is the multiplicative product of multiple independent random variables, it can be approximated using a lognormal distribution by considering the central limit theorem in the log domain, which is similar to the lognormal shadowing effect in classical wireless communications:

$$f_{\rho}(\rho) = \frac{1}{\rho\sigma_{\rho}\sqrt{2\pi}} e^{-\frac{\left(\ln\rho-\mu_{\rho}\right)^2}{2\sigma_{\rho}^2}}. \tag{3}$$

The two parameters μ_{ρ} and σ_{ρ} are, respectively, the mean and standard deviation of $\ln\rho$. In addition, the drug clearance rate describes how fast the drug is filtered out of the blood. The clearance is often modeled as a constant for a specific biological system.

It is worth emphasizing that the model in (2) is concise with a small number of unknown parameters, which is advantageous from the channel estimation perspective but may miss out on some useful details about the vascular network. Thus, it is important for the TDD system designer to achieve a balanced trade-off between channel model accuracy and estimation efficiency.

C. Out-messaging Interface Model

CMI can be employed as the out-messaging interface to estimate the total administered dose being deposited in the tumor. The cargo attached to nanorobots is a microwave contrast agent such as carbon nanotubes, ferroelectric nanoparticles, or magnetic nanoparticles, which can also be employed as a therapeutic agent [13], [15], [20]–[22]. The contrast agent alters the dielectric property of the targeted

tissue. Differential microwave imaging can then be applied to monitor backscatter signature over time, which images temporal variation in tissue anomaly and provides information on the therapeutic index of various nanoparticles in tumor. For illustration, breast cancer imaging is considered in the current work, where a schematic diagram of the CMI system is shown in Fig. 2. The same figure also shows a tumorous lesion buried in a cluttered background medium generated by tissue inhomogeneities.

Firstly, a single-pole Cole-Cole model is employed to describe the frequency dependence of the complex permittivity, $\varepsilon_{\text{breast}}$, of healthy breast tissue background medium over the band of interest (100 MHz to 20 GHz) [23]:

$$\varepsilon_{\text{breast}}(\omega) = F_1 + \frac{F_2}{1 + (j\omega F_3)^{1-F_4}} + \frac{F_5}{j\omega\varepsilon_0}, \tag{4}$$

where ω is the frequency in radian, ε_0 is the permittivity of free space, and $F_1 \sim F_5$ are fitting parameters. Secondly, in terms of tumor permittivity, $\varepsilon_{\text{tumor}}$, it has been shown that there is a large variation in the dielectric contrast between malignant and healthy breast tissues due to substantial heterogeneity and the contrast ranges from no more than 10% to fivefold [24]. Furthermore, the complex permittivity of tumor penetrated by nanorobots and attached with contrast medium nanocomposites can be approximated by applying the classical Maxwell Garnett equation [25]:

$$\tilde{\varepsilon}_{\text{tumor}}(\omega) = \varepsilon_{\text{tumor}}(\omega)\frac{[\varepsilon_{\text{agent}}(\omega) + 2\varepsilon_{\text{tumor}}(\omega)] + 2V_{\text{agent}}\,[\varepsilon_{\text{agent}}(\omega) - \varepsilon_{\text{tumor}}(\omega)]}{[\varepsilon_{\text{agent}}(\omega) + 2\varepsilon_{\text{tumor}}(\omega)] - V_{\text{agent}}\,[\varepsilon_{\text{agent}}(\omega) - \varepsilon_{\text{tumor}}(\omega)]}, \tag{5}$$

where $\tilde{\varepsilon}_{\text{tumor}}$ is the effective dielectric constant of tumor resulting from the inclusion of a volume fraction V_{agent} of contrast agent nanoparticles with dielectric constant $\varepsilon_{\text{agent}}$.

The next step is to derive the waveforms scattered by tumor. It is assumed that the antennas are immersed in a coupling medium with dielectric property matching the breast permittivity over the entire frequency band [15]. Consider a tumor oriented parallel to multiple spatially diverse monostatic antenna elements (i.e., the transmitter and receiver are collocated), $A_1, A_2, \cdots, A_Z$, generating equal electric current line sources, $i(t)$. The distances between the antennas and the tumor are $r_1 < r_2 < \cdots < r_Z$ as shown in Fig. 2. In the absence of a skin layer, the frequency-domain expression of the backscatter field at A_z $(z = 1, 2, \cdots, Z)$ is [26]:

$$I(\omega)\left[\frac{\omega\mu_0}{4}\sum_{\nu=-\infty}^{+\infty}\mathcal{K}_\nu(\omega)\mathcal{H}_\nu^{(2)}\left(k_{\text{breast}}r_z\right)\right], \tag{6}$$

where

$$\mathcal{K}_\nu(\omega) = \frac{\mathcal{J}_\nu'\left(\frac{k_{\text{breast}}d_{\text{tumor}}}{2}\right)\mathcal{J}_\nu\left(\frac{\tilde{k}_{\text{tumor}}d_{\text{tumor}}}{2}\right) - \sqrt{\frac{\tilde{\varepsilon}_{\text{tumor}}(\omega)}{\varepsilon_{\text{breast}}(\omega)}}\mathcal{J}_\nu\left(\frac{k_{\text{breast}}d_{\text{tumor}}}{2}\right)\mathcal{J}_\nu'\left(\frac{\tilde{k}_{\text{tumor}}d_{\text{tumor}}}{2}\right)}{\sqrt{\frac{\tilde{\varepsilon}_{\text{tumor}}(\omega)}{\varepsilon_{\text{breast}}(\omega)}}\mathcal{H}_\nu^{(2)}\left(\frac{k_{\text{breast}}d_{\text{tumor}}}{2}\right)\mathcal{J}_\nu'\left(\frac{\tilde{k}_{\text{tumor}}d_{\text{tumor}}}{2}\right) - \mathcal{H}_\nu^{(2)'}\left(\frac{k_{\text{breast}}d_{\text{tumor}}}{2}\right)\mathcal{J}_\nu\left(\frac{\tilde{k}_{\text{tumor}}d_{\text{tumor}}}{2}\right)}. \tag{7}$$

The term μ_0 is the permeability of free space, I is the frequency-domain representation of the current source, $\mathcal{H}_\nu^{(2)}$ is the ν^{th}-order Hankel function of the second kind, and $\mathcal{J}_\nu$ is the ν^{th}-order Bessel function. The prime $(')$ denotes a derivative with respect to the argument of the function, d_{tumor} is the diameter of the tumor, and k_{breast} and $\tilde{k}_{\text{tumor}}$ are the wavenumbers for the tissue background medium and the tumor mixed with nanoparticles, respectively. The propagation effects of a plane wave in the skin for the round-trip distances traveled are separately accounted for. To include a skin layer with relative dielectric constant $\varepsilon_{\text{skin}}$ and conductivity σ_{skin}, the slab model is applied where the skin response is given by [27]:

$$H_{\text{skin}}(\omega) = \left\{ \frac{\left[1 - R_{\text{skin}}^2(\omega)\right] e^{-j[k_{\text{skin}}(\omega) - k_{\text{breast}}(\omega)]\xi_{\text{skin}}}}{1 - R_{\text{skin}}^2(\omega) e^{-j2k_{\text{skin}}(\omega)\xi_{\text{skin}}}} \right\}^2 . \tag{8}$$

The term R_{skin} is the Fresnel reflection coefficient of single reflection exterior to the skin layer, ξ_{skin} is the thickness of the skin, and k_{skin} is the wavenumber for skin. Subsequently, time-domain backscatter signals are obtained from (6) and (8) by performing an inverse Fourier transform for a set of frequencies spanning the band of interest:

$$\begin{aligned} o_{\text{tumor}}(t) &= \mathbb{F}^{-1}\left\{ I(\omega) \left[\frac{\omega\mu_0}{4} \sum_{\nu=-\infty}^{+\infty} \mathcal{K}_\nu(\omega) \mathcal{H}_\nu^{(2)}\left(k_{\text{breast}} r_z\right) \right] H_{\text{skin}}(\omega) \right\} \\ &= \mathbb{F}^{-1}\left\{ I(\omega) H_{\text{tumor}}(\omega) \right\}, \end{aligned} \tag{9}$$

where H_{tumor} is the frequency-domain channel response due to tumor and $\mathbb{F}^{-1}$ denotes inverse Fourier transform. The backscatter signal due to tissue inhomogeneity can be obtained in a similar manner by replacing the tumor dielectric properties with the tissue heterogeneity dielectric constant and conductivity.

Finally, it is important to determine the relationship between the agent concentration at the host, x_{R} in (2), and the volume fraction V_{agent} in (5). Let D_{agent} and M_{agent} denote, respectively, the density and mass of agent nanoparticles. Let $\mathbb{V}_{\text{tumor}}$ denote the tumor volume. It can be easily shown that M_{agent}, which is proportional to x_{R}, is given by $M_{\text{agent}} = D_{\text{agent}} \frac{\mathbb{V}_{\text{tumor}} V_{\text{agent}}}{1 - V_{\text{agent}}}$. Consequently, in the real-life situation of $V_{\text{agent}} \ll 1$, x_{R} is proportional to V_{agent}, which in turn determines the effective dielectric constant of tumor $\tilde{\varepsilon}_{\text{tumor}}$ and the received backscatter signal $o_{\text{tumor}}(t)$ in (9). Hence, by monitoring the variation of $o_{\text{tumor}}(t)$ over time due to drug deposition and elimination, the touchable communication channel represented by the input-output relationship in (2) can be estimated as to be discussed in the following section.

III. Estimation of TDD Pharmocokinetic Model

A. Estimation of Contrast Agent Concentration

The information-theoretic-criteria-based tumor detection algorithm in [15] is revisited here in the current problem setting. Let $i_z(t)$ and $o_z(t)$ denote, respectively, the continuous-time excitation current and the overall signal received by A_z. Note that o_z includes both the tumor response $o_{\text{tumor},z}$ given by (9) and the tissue inhomogeneity response at A_z. In the frequency domain, the following general relationship can be obtained:

$$o_z(t) = \int_0^{T_{\text{sc},z}} h_z(\tau) i_z(t-\tau) d\tau + w_z(t), \tag{10}$$

where h_z is the continuous channel response, w_z is the additive white Gaussian noise, and $T_{\text{sc},z}$ is the length of the scattering channel. Sampling the received signal at rate f_0 and defining the following notations $o_z(m) = o_z(m/f_0)$, $i_z(m) = i_z(m/f_0)$, and $w_z(m) = w_z(m/f_0)$, the following discrete representation is obtained:

$$o_z(m) = \sum_{l=0}^{L_z-l} h_z(l) i_z(m-l) + w_z(m), \tag{11}$$

where $h_z(l)$ denotes the discrete channel response of $h_z(l/f_0)$ and L_z denotes the order of the discrete channel. Eq. (11) can be rewritten in the matrix form as

$$\mathbf{o}_z = \mathbf{H}_z \mathbf{i}_z + \mathbf{w}_z, \tag{12}$$

where

$$\mathbf{o}_z = [o_z((n-1)(L_z+M_z-1)+1) \ \cdots \ o_z(n(L_z+M_z-1))]^T, \tag{13}$$

$$\mathbf{H}_z = \begin{bmatrix} & & & h_z(0) \\ & & h_z(0) & h_z(1) \\ & \iddots & \vdots & \vdots \\ h_z(0) & h_z(1) & \cdots & h_z(M_z-1) \\ h_z(1) & h_z(2) & \cdots & h_z(M_z) \\ \vdots & \vdots & \iddots & \\ h_z(L_z-2) & h_z(L_z-1) & & \\ h_z(L_z-1) & & & \end{bmatrix}, \tag{14}$$

$$\mathbf{i}_z = [i_z(nM_z) \ \cdots \ i_z((n-1)M_z+1)]^T, \tag{15}$$

$$\mathbf{w}_z = [w_z((n-1)(L_z+M_z-1)+1) \ \cdots \ w_z(n(L_z+M_z-1))]^T. \tag{16}$$

In (13)-(16), $n = 1, 2, \cdots, N$ is the index of each observation, M_z is the signal length, and $\mathbf{o}_z$, $\mathbf{H}_z$, $\mathbf{i}_z$, and $\mathbf{w}_z$ are the observation vector, the channel matrix, the source signal vector, and the noise vector, respectively. The symbol $(^T)$ denotes matrix transpose.

Suppose that the delay introduced by a tumor is ℓ_z/f_0 $(0 < \ell_z \leq L_z - 1)$. the early-time responses caused by healthy tissue heterogeneities that yield time-of-arrival less than ℓ_z/f_0 can be distinguished from the late-time responses due to the cancer itself, healthy tissue inhomogeneities, as well as mutual interference between the cancer and other scattering centers with time-of-arrival no less than ℓ_z/f_0. Drug deposition in the cancer will distort the scattering channel responses caused by changes in the tumor dielectric properties, and only the late responses will be influenced. The new channel matrix after infusion of contrast agent is given by

$$\tilde{\mathbf{H}}_z = \mathbf{H}_z + \Delta\mathbf{H}_z, \tag{17}$$

where the $(i,j)^{\text{th}}$ $(i = 1, 2, \cdots, L_z + M_z - 1; j = 1, 2, \cdots, M_z)$ entry of the perturbation matrix $\Delta\mathbf{H}_z$ is expressed as

$$\Delta\mathbf{H}_z[i,j] = \begin{cases} 0; & \text{if } \mathbf{H}_z[i,j] = 0 \\ 0; & \text{if } \mathbf{H}_z[i,j] = h_z(l) \text{ and } l < \ell_z \\ \Delta h_z(l); & \text{if } \mathbf{H}_z[i,j] = h_z(l) \text{ and } l \geq \ell_z \end{cases} \tag{18}$$

In (18), $\Delta h_z(l)$ is a nonzero term summarizing the overall perturbation effect introduced to the l^{th} tap of the scattering channel.

CMI relies upon the difference between the backscatter responses with and without contrast medium delivered to the cancer, viz.,

$$\begin{aligned} \Delta\mathbf{o}_z &= \tilde{\mathbf{o}}_z - \mathbf{o}_z \\ &= \tilde{\mathbf{H}}_z\mathbf{i}_z + \tilde{\mathbf{w}}_z - (\mathbf{H}_z\mathbf{i}_z + \mathbf{w}_z) \\ &= \Delta\mathbf{H}_z\mathbf{i}_z + \Delta\mathbf{w}_z, \end{aligned} \tag{19}$$

where $\tilde{\mathbf{w}}_z$ is the noise associated with the post-contrast scattered signals. Note that $\Delta\mathbf{w}_z = \tilde{\mathbf{w}}_z - \mathbf{w}_z$ is also an additive white Gaussian noise. A close examination of (18) reveals that the first ℓ_z rows of $\Delta\mathbf{H}_z$ $(z = 1, 2, \cdots, Z)$ are empty vectors. Apparently, $\text{rank}\,(\Delta\mathbf{H}_z) \leq \min(L_z + M_z - 1 - \ell_z, M_z) = M_z$ by noting that $L_z \geq \ell_z + 1$. If we assume that the matrix $\Delta\mathbf{H}_z$ is of full column rank and the covariance matrix $\mathbf{I}_z = \mathbb{E}\{\mathbf{i}_z(t)\mathbf{i}_z^\dagger(t)\}$, where $\mathbb{E}$ denotes expectation, is nonsingular for all z, the rank of the covariance matrix $\Delta\mathbf{\Psi}_z = \Delta\mathbf{H}_z\mathbf{I}_z\Delta\mathbf{H}_z^\dagger$ is M_z. The information-theoretic criteria such as the Akaike information criterion or the minimum description length [15] can thus be applied to estimate the signal-to-noise ratio (SNR) $\eta_z = \|\Delta\mathbf{H}_z\mathbf{i}_z\|^2 / \mathbb{E}\left\{\|\Delta\mathbf{w}_z\|^2\right\}$.

Essentially, when an antenna A_z is far away from the tumor and η_z is very low, the received differential signal $\Delta\mathbf{o}_z$ only consists of the noise samples. Therefore, the estimated rank of $\triangle\mathbf{\Psi}_z$ *via* the information-theoretic criteria should be zero. On the contrary, if A_z is near the tumor and η_z is sufficiently large, there will be residual non-zero entries in $\Delta\mathbf{H}_z$. Therefore, the number of signals will be larger than zero. Subsequently, at any observation time t, we identify the antenna index $z^*(t)$ such that:

$$z^*(t) = \max\left\{z(t) \in \{1, 2, \cdots, Z\} : \text{rank}\left(\triangle\mathbf{\Psi}_{z(t)}\right) > 0\right\}. \tag{20}$$

The corresponding normalized SNR is obtained as:

$$\begin{aligned}\bar{\eta}_{z^*(t)} &= \frac{r_{z^*(t)}\eta^*}{r_{z^*(0)}\eta^*} \\ &= \frac{r_{z^*(t)}}{r_{z^*(0)}},\end{aligned} \tag{21}$$

where η^* represents the threshold SNR below which the CMI system is unable to detect the tumor. The two terms $r_{z^*(t)}$ and $r_{z^*(0)}$ are the distances from the tumor to antennas $A_{z^*(t)}$ and $A_{z^*(0)}$, respectively, where time 0 denotes the initial instant when nanorobots have just arrived at the tumor. These two factors compensate for radial spreading resulting in decrease in amplitude of an electromagnetic wave as it expands.

Finally, the normalized SNR $\bar{\eta}_{z^*(t)}$ increases monotonically with the time-varying volume fraction $V_{\text{agent}}(t)$ [see also (5)]. Instead of using the exact but complex relationship between $\bar{\eta}_{z^*(t)}$ and $V_{\text{agent}}(t)$ as presented in the previous section, the following simple yet versatile function is considered:

$$\bar{\eta}_{z^*(t)} = \left[\frac{V_{\text{agent}}(t)}{V_{\text{agent}}(0)}\right]^{\kappa} [\theta(t) - \theta(t-1)], \tag{22}$$

where $V_{\text{agent}}(0)$ is the volume fraction at the initial time 0 and $\theta(\cdot)$ is the Heaviside step function. For $\kappa \to \infty$, Eq. (22) describes the case that $\bar{\eta}_{z^*(t)}$ is more sensitive to $V_{\text{agent}}(t)$ in the large volume fraction regime. The case when $\bar{\eta}_{z^*(t)}$ varies more significantly with $V_{\text{agent}}(t)$ at low volume fraction is given by $\kappa \to 0$.

As the information-theoretic method was successfully applied to more complicated breast phantoms for tumor detection in [15], it is expected that the methodology would be applicable to a wide variety of breast models for estimation of contrast agent concentration.

B. Estimation of Pharmocokinetic Model

Estimation of the pharmocokinetic model is achieved by sending Q impulses of contrast agent nanoparticle and measuring the corresponding pilot channel responses at the tumor in terms of volume fraction.

The volume fraction at the initial time $V_{\text{agent}}(0)$ is proportional to the path loss ρ in (2) in the practical scenario of $V_{\text{agent}}(0) \ll 1$. Therefore, following (2), for the q^{th} $(q = 1, 2, \cdots, Q)$ probing impulse, its response in terms of volume fraction can be expressed as:

$$V_{\text{agent},q}(t) = V_{\text{agent},q}(0)e^{-\zeta t} + \text{noise}, \tag{23}$$

where the subscript q denotes the model parameters for the q^{th} impulse. In order to weight the measurement points equally in least squares fitting, the objective is to minimize the function:

$$\sum_{p=1}^{P} V_{\text{agent},q}(t_p) \left[\ln V_{\text{agent},q}(t_p) - \ln V_{\text{agent},q}(0) + \zeta t_p\right]^2 \tag{24}$$

over P measurement times for any q, which yields the following solutions [28]:

$$\begin{aligned}\ln \hat{V}_{\text{agent},q}(0) =& \frac{\sum_{p=1}^{P}\left[t_p^2 V_{\text{agent},q}(t_p)\right]\sum_{p=1}^{P}\left[V_{\text{agent},q}(t_p)\ln V_{\text{agent},q}(t_p)\right]}{\sum_{p=1}^{P} V_{\text{agent},q}(t_p)\sum_{p=1}^{P}\left[t_p^2 V_{\text{agent},q}(t_p)\right] - \left[\sum_{p=1}^{P} t_p V_{\text{agent},q}(t_p)\right]^2} \\ &- \frac{\sum_{p=1}^{P}\left[t_p V_{\text{agent},q}(t_p)\right]\sum_{p=1}^{P}\left[t_p V_{\text{agent},q}(t_p)\ln V_{\text{agent},q}(t_p)\right]}{\sum_{p=1}^{P} V_{\text{agent},q}(t_p)\sum_{p=1}^{P}\left[t_p^2 V_{\text{agent},q}(t_p)\right] - \left[\sum_{p=1}^{P} t_p V_{\text{agent},q}(t_p)\right]^2}\end{aligned} \tag{25}$$

and

$$\begin{aligned}\hat{\zeta}_q =& -\frac{\sum_{p=1}^{P} V_{\text{agent},q}(t_p)\sum_{p=1}^{P}\left[t_p V_{\text{agent},q}(t_p)\ln V_{\text{agent},q}(t_p)\right]}{\sum_{p=1}^{P} V_{\text{agent},q}(t_p)\sum_{p=1}^{P}\left[t_p^2 V_{\text{agent},q}(t_p)\right] - \left[\sum_{p=1}^{P} t_p V_{\text{agent},q}(t_p)\right]^2} \\ &+ \frac{\sum_{p=1}^{P}\left[t_p V_{\text{agent},q}(t_p)\right]\sum_{p=1}^{P}\left[V_{\text{agent},q}(t_p)\ln V_{\text{agent},q}(t_p)\right]}{\sum_{p=1}^{P} V_{\text{agent},q}(t_p)\sum_{p=1}^{P}\left[t_p^2 V_{\text{agent},q}(t_p)\right] - \left[\sum_{p=1}^{P} t_p V_{\text{agent},q}(t_p)\right]^2}.\end{aligned} \tag{26}$$

The symbol $(\hat{\cdot})$ denotes an estimated quantity. Note that as the drug elimination rate is a constant, the final least-squares estimate of ζ is obtained as:

$$\hat{\zeta} = \frac{1}{Q}\sum_{q=1}^{Q} \hat{\zeta}_q. \tag{27}$$

Similar to the path loss ρ, the volume fraction $V_{\text{agent}}(0)$ is also log-normally distributed. For determining the maximum likelihood estimator of the lognormal distribution parameters μ_V and σ_V for $V_{\text{agent}}(0)$, the log-likelihood function is written as:

$$\begin{aligned}&\mathcal{L}_{LN}\left(\mu_V, \sigma_V \middle| \hat{V}_{\text{agent},1}(0), \hat{V}_{\text{agent},2}(0), \cdots, \hat{V}_{\text{agent},Q}(0)\right) \\ &= -\sum_{q=1}^{Q} \ln \hat{V}_{\text{agent},q}(0) + \mathcal{L}_N\left(\mu_V, \sigma_V \middle| \ln \hat{V}_{\text{agent},1}(0), \ln \hat{V}_{\text{agent},2}(0), \cdots, \ln \hat{V}_{\text{agent},Q}(0)\right),\end{aligned} \tag{28}$$

where $\mathcal{L}_N$ denotes the log-likelihood function of a normal distribution. Since the first term in (28) is constant with regard to μ_V and σ_V, both logarithmic likelihood functions, $\mathcal{L}_{LN}$ and $\mathcal{L}_N$, reach their

maximum with the same μ_V and σ_V. Hence, using the formulas for the normal distribution maximum likelihood parameter estimators, for the log-normal distribution it holds that [29]:

$$\hat{\mu}_V = \frac{\sum_{q=1}^{Q} \ln \hat{V}_{\text{agent},q}(0)}{Q} \tag{29}$$

and

$$\hat{\sigma}_V^2 = \frac{\sum_{q=1}^{Q} \left[\ln \hat{V}_{\text{agent},q}(0) - \hat{\mu}_V\right]^2}{Q}. \tag{30}$$

IV. Optimization of Concentration-Time Profile of Injected Drug Molecules

Three waveform design strategies are proposed in this section to achieve minimum inter-symbol interference, maximum non-fade duration, and minimum BER. From the TDD perspective, these criteria yield low side-effects caused by residual drug after each therapeutic session, long duration when the drug dose is sufficiently high, and low rate that a therapeutic operation is interpreted wrongly at tumor, respectively.

For simplicity, we assume that $x_{\text{T}}(t)$ is a boxcar function given by $x_{\text{T}}(t) = \frac{1}{T_{\text{burst}}}\left[\theta(t) - \theta(t - T_{\text{burst}})\right]$. The output signal is computed as:

$$\begin{aligned} x_{\text{R}}(t) &= \begin{cases} \int_0^t \frac{\rho}{T_{\text{burst}}} \exp\left[-\zeta(t-\tau)\right] d\tau, & 0 \le t \le T_{\text{burst}} \\ \int_0^{T_{\text{burst}}} \frac{\rho}{T_{\text{burst}}} \exp\left[-\zeta(t-\tau)\right] d\tau, & t > T_{\text{burst}} \end{cases} \\ &= \begin{cases} \frac{\rho[1-\exp(-\zeta t)]}{\zeta T_{\text{burst}}}, & 0 \le t \le T_{\text{burst}} \\ \frac{\rho\{\exp[-\zeta(t-T_{\text{burst}})]-\exp(-\zeta t)\}}{\zeta T_{\text{burst}}}, & t > T_{\text{burst}} \end{cases} \end{aligned} \tag{31}$$

Therefore, the probability that $x_{\text{R}}(t)$ at the end of each symbol duration, $t = T_{\text{slot}}$, is no greater than a specified threshold x_{ISI} is derived as:

$$\begin{aligned} P_{\text{ISI}} &= \Pr\left\{x_{\text{R}}(T_{\text{slot}}) \le x_{\text{ISI}}\right\} \\ &= \Pr\left\{\rho \le \frac{\zeta T_{\text{burst}} x_{\text{ISI}}}{\exp\left[-\zeta\left(T_{\text{slot}} - T_{\text{burst}}\right)\right] - \exp\left(-\zeta T_{\text{slot}}\right)}\right\} \\ &= \frac{1}{2} + \frac{1}{2}\text{erf}\left\{\frac{\ln\left\{\frac{\zeta T_{\text{burst}} x_{\text{ISI}}}{\exp[-\zeta(T_{\text{slot}}-T_{\text{burst}})]-\exp(-\zeta T_{\text{slot}})}\right\} - \mu_\rho}{\sqrt{2}\sigma_\rho}\right\}, \end{aligned} \tag{32}$$

by noting that $T_{\text{slot}} > T_{\text{burst}}$ and ρ follows a lognormal distribution as expressed in (3). The term $\text{erf}\{\cdot\}$ denotes the error function and the subscript ISI indicates that the threshold is related to: inter-symbol interference.

Subsequently, provided with another threshold x_{NFD} and following (32), the duration when the contrast agent concentration is above x_{NFD} at each symbol time is expressed as

$$\begin{aligned}\Delta t &= t_u\left(x_{\mathrm{NFD}}\right) - t_l\left(x_{\mathrm{NFD}}\right) \\ &= -\frac{1}{\zeta}\ln\left\{\frac{\zeta T_{\mathrm{burst}} x_{\mathrm{NFD}}}{\rho\left[\exp\left(\zeta T_{\mathrm{burst}}\right)-1\right]}\right\} - \left[-\frac{1}{\zeta}\ln\left(1-\frac{\zeta T_{\mathrm{burst}} x_{\mathrm{NFD}}}{\rho}\right)\right] \\ &= \frac{1}{\zeta}\ln\left\{\frac{\left[\exp\left(\zeta T_{\mathrm{burst}}\right)-1\right]\left(\rho-\zeta T_{\mathrm{burst}} x_{\mathrm{NFD}}\right)}{\zeta T_{\mathrm{burst}} x_{\mathrm{NFD}}}\right\},\end{aligned} \tag{33}$$

where t_u and t_l are the intersections of the straight line $x_{\mathrm{R}}(t) = x_{\mathrm{NFD}}$ and the curve drawn from (31). The subscript NFD indicates that the threshold is related to non-fade duration. By applying (33) and (3), the probability that Δt is no less than a threshold Δt_{NFD} is given by:

$$\begin{aligned}P_{\mathrm{NFD}} &= \Pr\left\{\Delta t \geq \Delta t_{\mathrm{NFD}}\right\} \\ &= \Pr\left\{\rho \geq \frac{\zeta T_{\mathrm{burst}} x_{\mathrm{NFD}} \exp\left(\zeta \Delta t_{\mathrm{NFD}}\right)}{\exp\left(\zeta T_{\mathrm{burst}}\right)-1} + \zeta T_{\mathrm{burst}} x_{\mathrm{NFD}}\right\} \\ &= \frac{1}{2} - \frac{1}{2}\mathrm{erf}\left\{\frac{\ln\left\{\frac{\zeta T_{\mathrm{burst}} x_{\mathrm{NFD}} \exp\left(\zeta \Delta t_{\mathrm{NFD}}\right)}{\exp\left(\zeta T_{\mathrm{burst}}\right)-1} + \zeta T_{\mathrm{burst}} x_{\mathrm{NFD}}\right\} - \mu_\rho}{\sqrt{2}\sigma_\rho}\right\}.\end{aligned} \tag{34}$$

A. Maximization of P_{ISI} and P_{NFD}

The inter-symbol interference and non-fade duration criteria for the touchable communication waveform design aim at finding the values of T_{burst} such that P_{ISI} and P_{NFD} in (32) and (34) are maximized.

In the situation that there is a tradeoff between P_{ISI} and P_{NFD}, the Pareto efficiency can be applied. It is a concept in multi-criteria optimization enabling all tradeoffs among the best combinations of multiple criteria to be evaluated. The objective here is to maximize P_{ISI} and P_{NFD} simultaneously, and the Pareto frontier is defined as the set of choices of $(P_{\mathrm{ISI}}, P_{\mathrm{NFD}})$ whereby any improvement with respect to P_{ISI} comes at the expense of P_{NFD}. Each point along that frontier represents a unique parameterization of the transmitted signal $x_{\mathrm{T}}(t)$ in terms of its pulse duration T_{burst}, so the associated Pareto optimality identifies multiple Pareto solutions of $(P_{\mathrm{ISI}}, P_{\mathrm{NFD}})$. Through this procedure one is able to investigate differences among the multiple solutions that are able to optimize varying combinations of the two assessment criteria.

The aforementioned Pareto efficiency strategy for waveform design can be formally expressed as follows. Consider the system with function $\mathcal{F}: \mathbb{R}_{[0,T_{\mathrm{slot}}]} \rightarrow \mathbb{R}^2_{[0,1]}$, where $\mathbb{X}$ is a compact set of feasible decisions of T_{burst} in the space $\mathbb{R}_{[0,T_{\mathrm{slot}}]} = \{x \in \mathbb{R} | 0 \leq x \leq T_{\mathrm{slot}}\}$ and $\mathbb{Y}$ is the feasible set of criterion vectors $(P_{\mathrm{ISI}}, P_{\mathrm{NFD}})$ in $\mathbb{R}^2_{[0,1]} = \{y \in \mathbb{R} | 0 \leq y \leq 1\} \times \{y \in \mathbb{R} | 0 \leq y \leq 1\}$. Larger criteria values are

preferred to smaller ones. A point $y'' \in \mathbb{R}^2_{[0,1]}$ is preferred to (strictly dominates) another point $y' \in \mathbb{R}^2_{[0,1]}$, written as $y'' \succ y'$. The Pareto frontier is thus written as:

$$\left\{y' \in \mathbb{Y} : \left\{y'' \in \mathbb{Y} : y'' \succ y', y'' \neq y'\right\} = \varnothing\right\}. \tag{35}$$

The Pareto optimum criterion aims at finding the set of T_{burst} such that the Pareto frontier is achieved.

B. Minimization of BER

As described in Section II-A, bits '1' and '0' are represented by a burst of drug molecules within a time slot and the absence of molecules, respectively. It is thus assumed that the event of an erroneous bit occurs under the following two conditions. When a bit '0' is transmitted, the receiver (tumor) detects the bit to be '1' if the duration when the drug concentration is above x_{NFD} is no less than Δt_{NFD} within the symbol time. On the other hand, a bit '1' is incorrectly detected as '0' if this duration is less than Δt_{NFD}.

Subsequently, by ignoring counting errors at the receiver (i.e., all drug molecules delivered by nanorobots to the tumor will be bound to cancer cell receptors), the BER can be derived as

$$\begin{aligned} P_e &= \Pr\left\{\hat{b}_j = 1 \middle| b_j = 0\right\} \Pr\left\{b_j = 0\right\} + \Pr\left\{\hat{b}_j = 0 \middle| b_j = 1\right\} \Pr\left\{b_j = 1\right\} \\ &\approx \Pr\left\{\hat{b}_j = 1 \middle| b_j = 0; b_{j-1} = 1\right\} \Pr\left\{b_j = 0\right\} \Pr\left\{b_{j-1} = 1\right\} \\ &\quad + \Pr\left\{\hat{b}_j = 0 \middle| b_j = 1; b_{j-1} = 0\right\} \Pr\left\{b_j = 1\right\} \Pr\left\{b_{j-1} = 0\right\} \\ &\quad + \Pr\left\{\hat{b}_j = 0 \middle| b_j = 1; b_{j-1} = 1\right\} \Pr\left\{b_j = 1\right\} \Pr\left\{b_{j-1} = 1\right\}, \end{aligned} \tag{36}$$

where b_j denotes the j^{th} bit and $\Pr\{\cdot|\cdot\}$ is the conditional probability. Eq. (36) assumes that only the $(j-1)^{\text{th}}$ bit has impact on the detection of the j^{th} bit, because the concentration-time profiles for earlier bits decay quickly with time.

The event $\left\{\hat{b}_j = 1 \middle| b_j = 0; b_{j-1} = 1\right\}$ occurs when the inter-symbol interference due to the $(j-1)^{\text{th}}$ bit is above a certain value, resulting in the duration when the drug concentration is above x_{NFD} at the j^{th} bit is no less than Δt_{NFD}, i.e.,

$$\begin{aligned} & t_u\left(x_{\text{NFD}}\right) - T_{\text{slot}} \geq \Delta t_{\text{NFD}} \\ \Rightarrow & -\frac{1}{\zeta} \ln\left\{\frac{\zeta T_{\text{burst}} x_{\text{NFD}}}{\rho\left[\exp\left(\zeta T_{\text{burst}}\right) - 1\right]}\right\} - T_{\text{slot}} \geq \Delta t_{\text{NFD}} \\ \Rightarrow & \rho \geq \frac{\zeta T_{\text{burst}} x_{\text{NFD}}}{\left[\exp\left(\zeta T_{\text{burst}}\right) - 1\right] \exp\left[-\zeta\left(T_{\text{slot}} + \Delta t_{\text{NFD}}\right)\right]}. \end{aligned} \tag{37}$$

Consequently, the following conditional probability is given by

$$\Pr\left\{\hat{b}_j = 1 \middle| b_j = 0; b_{j-1} = 1\right\} = \Pr\left\{\rho \geq \frac{\zeta T_{\text{burst}} x_{\text{NFD}}}{\left[\exp\left(\zeta T_{\text{burst}}\right) - 1\right] \exp\left[-\zeta\left(T_{\text{slot}} + \Delta t_{\text{NFD}}\right)\right]}\right\} = \frac{1}{2} - \frac{1}{2}\text{erf}\left\{\frac{\ln\left\{\frac{\zeta T_{\text{burst}} x_{\text{NFD}}}{\left[\exp(\zeta T_{\text{burst}})-1\right] \exp\left[-\zeta(T_{\text{slot}}+\Delta t_{\text{NFD}})\right]}\right\} - \mu_\rho}{\sqrt{2}\sigma_\rho}\right\}. \tag{38}$$

Furthermore, the event $\left\{\hat{b}_j = 0 \middle| b_j = 1; b_{j-1} = 0\right\}$ is complementary to the non-fade event in (34) because there is no inter-symbol interference from the $(j-1)^{\text{th}}$ bit. Thus,

$$\Pr\left\{\hat{b}_j = 0 \middle| b_j = 1; b_{j-1} = 0\right\} = 1 - P_{\text{NFD}}. \tag{39}$$

Next, the event $\left\{\hat{b}_j = 0 \middle| b_j = 1; b_{j-1} = 1\right\}$ occurs when the summation of the residual drug molecules from the $(j-1)^{\text{th}}$ bit and the drug entering the tumor for the j^{th} bit is too low to achieve correct detection of bit 1. The two time instants when the drug concentration is equal to x_{NFD} are first calculated by applying (31) and assuming that the propagation channels for two consecutive bits are fully correlated. For $T_{\text{slot}} \leq t_l \leq T_{\text{slot}} + T_{\text{burst}}$, the following relationship is satisfied:

$$\frac{\rho\left\{\exp\left[-\zeta\left(t_l - T_{\text{burst}}\right)\right] - \exp\left(-\zeta t_l\right)\right\}}{\zeta T_{\text{burst}}} + \frac{\rho\left[1 - \exp\left[-\zeta\left(t_l - T_{\text{burst}}\right)\right]\right]}{\zeta T_{\text{burst}}} = x_{\text{NFD}}, \tag{40}$$

resulting in

$$t_l = -\frac{1}{\zeta}\ln\left(1 - \frac{\zeta T_{\text{burst}} x_{\text{NFD}}}{\rho}\right). \tag{41}$$

On the other hand, for $T_{\text{slot}} + T_{\text{burst}} < t_u \leq 2T_{\text{slot}}$, we have

$$\frac{\rho\left\{\exp\left[-\zeta\left(t_u - T_{\text{burst}}\right)\right] - \exp\left(-\zeta t_u\right)\right\}}{\zeta T_{\text{burst}}} + \frac{\rho\left\{\exp\left[-\zeta\left(t_u - 2T_{\text{burst}}\right)\right] - \exp\left[-\zeta\left(t_u - T_{\text{burst}}\right)\right]\right\}}{\zeta T_{\text{burst}}} = x_{\text{NFD}}, \tag{42}$$

giving rise to

$$t_u = -\frac{1}{\zeta}\ln\left\{\frac{\zeta T_{\text{burst}} x_{\text{NFD}}}{\rho\left[\exp\left(2\zeta T_{\text{burst}}\right) - 1\right]}\right\}. \tag{43}$$

By applying the similar approach to (33) and (34), the following conditional probability is obtained:

$$\Pr\left\{\hat{b}_j = 0 \middle| b_j = 1; b_{j-1} = 1\right\} = \Pr\left\{\rho \leq \frac{\zeta T_{\text{burst}} x_{\text{NFD}} \exp\left(\zeta \Delta t_{\text{NFD}}\right)}{\exp\left(2\zeta T_{\text{burst}}\right) - 1} + \zeta T_{\text{burst}} x_{\text{NFD}}\right\} = \frac{1}{2} + \frac{1}{2}\text{erf}\left\{\frac{\ln\left\{\frac{\zeta T_{\text{burst}} x_{\text{NFD}} \exp(\zeta \Delta t_{\text{NFD}})}{\exp(2\zeta T_{\text{burst}})-1} + \zeta T_{\text{burst}} x_{\text{NFD}}\right\} - \mu_\rho}{\sqrt{2}\sigma_\rho}\right\}. \tag{44}$$

Substituting (38), (39), and (44) into (36) yields the closed-form expression of BER.

Finally, the BER criterion for the touchable communication waveform design aims at finding the optimal value of T_{burst} such that the BER in (36) is minimized.

Because the contrast agent concentration is proportional to the volume fraction and only the latter is estimated through the CMI system, the volume fraction will be used during the waveform design process.

V. Numerical Results and Analysis

A. System Settings for Simulation Study

A study case of CMI for optimal targeted therapies is presented in this section by applying the proposed communication waveform design strategies. The CMI of breast cancer is investigated as illustrated in Fig. 2. A single $1\ \mathrm{cm}$ diameter cancerous mass is placed in the breast with multiple tissue inhomogeneities. The dielectric properties of healthy breast tissues are governed by (4), where the "fat-medium" category in [23] is considered with the following model parameters: $F_1 = 3.140$, $F_2 = 1.708$, $F_3 = 14.65\ \mathrm{ps}$, $F_4 = 0.061$, and $F_5 = 0.036\ \mathrm{S/m}$. The dielectric values of tumor tissue are assumed to be fivefold those of healthy tissue across the whole band of interest [15], [24]. To emulate an uptake of contrast agent nanoparticles in malignant tissue, the complex permittivity of the inclusion vary with the volume fraction of drug molecules by following the mixture formula in (5). The contrast agent nanoparticles are assumed to have exceptionally high microwave-frequency dielectric properties such as the functionalizing CVD-synthesized carbon nanotubes *via* sonication in nitric and sulfuric acid investigated in [14]. The real and imaginary parts of the complex permittivity of the agent are assumed to be 200 and 100, respectively, over the band of interest [30]. The numerical phantom includes a skin layer with relative permittivity 36.0 and conductivity $4.0\ \mathrm{S/m}$ [26]. The thickness of the skin layer is $0.2\ \mathrm{cm}$.

It is further assumed that antennas are immersed in a coupling medium with dielectric property matching the breast permittivity over the entire frequency band [26], which can be achieved by using various tissue-mimicking materials. The imaging system is comprised of an array of 41 elements located at $2\ \mathrm{cm} \sim 42\ \mathrm{cm}$ from the tumor in an interval of $1\ \mathrm{cm}$. Each antenna is driven with a modulated Gaussian monocycle with the modulation frequency $1\ \mathrm{GHz}$ and pulse width $120\ \mathrm{ps}$ [15], [26]. The reflected waveform is recorded at the same antenna (monostatic configuration). The backscatter signals received at the antennas are computed by applying (9). The accumulation of drug molecules in the tumor follows the input-output relationship in (2) and the corresponding impulse response in terms of volume fraction is given by (23). It is supposed that the mean and standard deviation of the natural logarithm of path loss from the injection site to the tumor are $\ln 0.2$ and 0.2, respectively. We consider three different elimination rates: $\zeta = 1.3\ \mathrm{day}^{-1}$, $1.5\ \mathrm{day}^{-1}$, and $1.7\ \mathrm{day}^{-1}$ [18]. The difference between the postcontrast and precontrast signals is then computed for various concentrations of nanoparticles. This clean differential waveform is first corrupted by a multiplicative complex Gaussian vector process

representing measurement uncertainties. Subsequently, an additive white Gaussian noise vector is added to the artifact-corrupted differential signal. The algorithm presented in Section III is then applied to estimate the normalized SNR at each antenna and the time-varying volume fraction of drug molecules.

The final step is to determine the desirable values of $T_{\rm burst}$ for optimal targeted therapies by employing the inter-symbol interference, non-fade duration, and BER waveform design criteria in Section IV.

B. Numerical Results

The dielectric constant and conductivity of tumor mixed with various volume fractions of drug molecules are shown in Fig. 3. Both the dielectric properties increase with volume fraction. On the other hand, the dielectric constant decreases and the conductivity increases as the frequency increases. Fig. 4 depicts the relationships between the normalized SNR $\bar{\eta}_{z^*(t)}$ and the normalized volume fraction $V_{\rm agent}(t)/V_{\rm agent}(0)$ by applying the exact formulation in Section II-C and the approximation in (22) with $\kappa = 1.75$, respectively. The approximation matches well the exact solution throughout the entire range of $V_{\rm agent}(t)/V_{\rm agent}(0)$.

Fig. 5 plots the relationships between the estimated rank of $\Delta\mathbf{\Psi}_z$ in (20) and the SNR of differential signal by utilizing the Akaike information criterion and the maximum description length, respectively. As can be seen from this figure, the rank decreases as SNR reduces and the threshold SNRs can be obtained when the rank has just turned to zero, which verifies the effectiveness of the algorithm presented in (20) and (21). It is worth noting that the Akaike information criterion is more sensitive than the maximum description length at the low SNR regime.

Fig. 6 shows 10 independent pilot channel responses measured by the CMI system. Due to the discrete structure of the antenna array, the impulse responses are discretized as well. Also shown are the exact mean response with $\mu_V = \ln 0.2$ and $\zeta = 1.5$ and the estimated mean response with $\hat{\mu}_V = \ln 0.204$ and $\hat{\zeta} = 1.5035$. As demonstrated in Fig. 6, the exact model parameters of the lognormal distribution and exponential clearance agree well with the estimated values. Furthermore, the estimated standard deviation is $\hat{\sigma}_V = 0.1924$, which is very close to the exact value of $\sigma_V = 0.2$.

The relationships between $P_{\rm ISI}$, $P_{\rm NFD}$, and $T_{\rm burst}$ for various values of drug clearance rate ζ are depicted in Fig. 7. As shown in this figure, as ζ decreases, $P_{\rm ISI}$ decreases leading to more severe inter-symbol interference. On the contrary, $P_{\rm NFD}$ increases with reduced ζ, indicating longer duration when the drug concentration is above a threshold level during each symbol time. In general, $P_{\rm ISI}$ decreases whereas $P_{\rm NFD}$ increases as $T_{\rm burst}$ increases.

The Pareto frontiers of $(P_{\rm ISI}, P_{\rm NFD})$ for various elimination rates are drawn in Fig. 8(a), which agree

with the trend observed in Fig. 7. The zoomed-in versions of Fig. 8(a) for $\zeta = 1.3\ \mathrm{day}^{-1}$, $\zeta = 1.5\ \mathrm{day}^{-1}$, and $\zeta = 1.7\ \mathrm{day}^{-1}$ are shown in Fig. 8(b)-(c), respectively. Noteworthily, in the regime of small P_{ISI} (less than ~ 0.002), P_{NFD} increases with P_{ISI} and the Pareto optimality does not exist. In this case, there is no tradeoff between these two probabilities and a single T_{burst} can be found to maximize both the probabilities simultaneously.

Finally, Fig. 9 demonstrates the relationships between BER and T_{burst} for various values of elimination rate ζ. It can be seen that overall, a larger ζ results in a larger BER, though there are some crossovers when T_{burst} approaches $1\ \mathrm{day}$. For all the clearance rates, the optimum T_{burst} that result in minimum BERs can be acquired. Moreover, the optimum T_{burst} increases with ζ.

VI. Conclusion

A novel model of CMI-assisted optimal TDD from the perspective of touchable communication channel estimation and waveform design has been proposed. The CMI technique has been employed as a pretherapeutic evaluation technique to determine the pharmacokinetic model, where an information-theoretic-criteria-based signal processing algorithm was applied to estimate drug accumulation in tumor. This step is analogous to the estimation of channel impulse response in the classical communication systems. Three TDD optimization strategies have been introduced. These strategies are based on minimization of residual drug molecules at the end of each therapeutic session (i.e., inter-symbol interference), maximization of duration that the drug intensity is above a prespecified threshold during each therapeutic session (i.e., non-fade duration), and minimization of average rate that a therapeutic operation is not received correctly at tumor (i.e., BER). Finally, comprehensive numerical examples have been presented to demonstrate the key processes and properties of the proposed analytical framework. The current work may provide useful insight on realistic and clinically relevant design and implementation of touchable communication systems for targeted therapies.

References

[1] O. M. Koo, I. Rubinstein, and H. Onyuksel, "Role of nanotechnology in targeted drug delivery and imaging: a concise review," *Nanomed.*, vol. 1, no. 3, pp. 193–212, Sep. 2005.

[2] O. Felfoul, M. Mohammadi, S. Taherkhani, and et al., "Magneto-aerotactic bacteria deliver drug-containing nanoliposomes to tumour hypoxic regions," *Nature Nanotechnology*, pp. 1–7, 2016, Advance Online Publication, DOI: 10.1038/NNANO.2016.137.

[3] L. Mellal, D. Folio, K. Belharet, and A. Ferreira, "Modeling of optimal targeted therapies using drug-loaded magnetic nanoparticles for the liver cancer," *IEEE Trans. Nanobiosci.*, vol. 15, no. 3, pp. 265–274, Apr. 2016.

[4] Y. Chahibi, M. Pierobon, S. O. Song, and I. F. Akyildiz, "A molecular communication system model for particulate drug delivery systems," *IEEE Trans. Biomed. Eng.*, vol. 60, no. 12, pp. 3468–3483, Dec. 2013.

[5] Y. Chahibi and I. F. Akyildiz, "Molecular communication noise and capacity analysis for particulate drug delivery systems," *IEEE Trans. Commun.*, vol. 62, no. 11, pp. 3891–3903, Nov. 2014.

[6] Y. Chahibi, I. F. Akyildiz, S. Balasubramaniam, and Y. Koucheryavy, "Molecular communication modeling of antibody-mediated drug delivery systems," *IEEE Trans. Biomed. Eng.*, vol. 62, no. 7, pp. 1683–1695, July 2015.

[7] Y. Chahibi, M. Pierobon, and I. F. Akyildiz, "Pharmacokinetic modeling and biodistribution estimation through the molecular communication paradigm," *IEEE Trans. Biomed. Eng.*, vol. 62, no. 10, pp. 2410–2420, Oct. 2015.

[8] Y. Chen, P. Kosmas, P. S. Anwar, and L. Huang, "A touch-communication framework for drug delivery based on a transient microbot system," *IEEE Trans. NanoBiosci.*, vol. 14, no. 4, pp. 397–408, June 2015.

[9] M. Femminella, G. Reali, and A. V. Vasilakos, "A molecular communications model for drug delivery," *IEEE Trans. Nanobiosci.*, vol. 14, no. 8, pp. 935–945, Dec. 2015.

[10] U. A. K. Chude-Okonkwo, R. Malekian, and B. T. Sunil Maharaj, "Molecular communication model for targeted drug delivery in multiple disease sites with diversely expressed enzymes," *IEEE Trans. Nanobiosci.*, vol. 15, no. 3, pp. 230–245, Apr. 2016.

[11] Y. Chen, T. Nakano, P. Kosmas, C. Yuen, A. V. Vasilakos, and M. Asvial, "Green touchable nanorobotic sensor networks," *IEEE Commun. Mag.*, pp. 136–142, Nov. 2016.

[12] T. Nakano, S. Kobayashi, T. Suda, Y. Okaie, Y. Hiraoka, and T. Haraguchi, "Externally controllable molecular communication," *IEEE J. Sel. Areas Commun.*, vol. 32, no. 12, pp. 2417–2431, Dec. 2014.

[13] A. Mashal, B. Sitharaman, X. Li, P. K. Avti, A. V. Sahakian, J. H. Booske, and S. C. Hagness, "Toward carbon-nanotube-based theranostic agents for microwave detection and treatment of breast cancer: Enhanced dielectric and heating response of tissue-mimicking materials," *IEEE Trans. Biomed. Eng.*, vol. 57, pp. 1831–1834, Aug. 2010.

[14] S. X. Xie, F. Gao, S. C. Patel, J. H. Booske, S. C. Hagness, and B. Sitharaman, "Clinically relevant CNT dispersions with exceptionally high dielectric properties for microwave theranostic applications," *IEEE Trans. Biomed. Eng.*, vol. 61, no. 11, pp. 2718–2723, 2014.

[15] Y. Chen and P. Kosmas, "Detection and localization of tissue malignancy using contrast-enhanced microwave imaging: Exploring information theoretic criteria," *IEEE Trans. Biomed. Eng.*, vol. 59, pp. 766–776, Mar. 2012.

[16] A. Ergun, K. Camphausen, and L. W. Wein, "Optimal scheduling of radiotherapy and angiogenic inhibitors," *Bulletin of Mathematical Biology*, vol. 65, no. 3, pp. 407–424, 2003.

[17] L. G. de Pillis, W. Gu, K. R. Fister, T. A. Head, K. Maples, A. Murugan, T. Neal, and K. Yoshida, "Chemotherapy for tumors: An analysis of the dynamics and a study of quadratic and linear optimal controls," *Mathematical Biosciences*, vol. 209, no. 1, pp. 292–315, 2007.

[18] P. Hahnfeldt, D. Panigrahy, J. Folkman, and L. Hlatky, "Tumor development under angiogenic signaling a dynamical theory of tumor growth, treatment response, and postvascular dormancy," *Cancer Research*, vol. 59, no. 19, pp. 4770–4775, 1999.

[19] Q. Zhou, P. Guo, G. D. Kruh, P. Vicini, X. Wang, and J. M. Gallo, "Predicting human tumor drug concentrations from a preclinical pharmacokinetic model of temozolomide brain disposition," *Cancer Therapy: Preclinical*, vol. 13, no. 14, pp. 4271–4279, 2007.

[20] Y. Chen, P. Kosmas, and S. Martel, "Microwave breast tumor detection and size estimation using contrast-agent-loaded magnetotactic bacteria," in *Proc. IEEE EMBC 2013*, Osaka, Japan, Jul. 2013.

[21] S. Semenov, N. Pham, and S. Egot-Lemaire, "Ferroelectric nanoparticles for contrast enhancement microwave tomography:

Feasibility assessment for detection of lung cancer," in *Proc. World Congress on Medical Physics and Biomedical Engineering*, Munich, Germany, Sep. 2009.

[22] G. Bellizzi, O. M. Bucci, and I. Catapano, "Microwave cancer imaging exploiting magnetic nanoparticles as contrast agent," *IEEE Trans. Biomed. Eng.*, vol. 58, pp. 2528–2536, Sept. 2011.

[23] E. Zastrow, S. K. Davis, M. Lazebnik, F. Kelcz, B. D. Van Veen, and S. C. Hagness, "Development of anatomically realistic numerical breast phantoms with accurate dielectric properties for modeling microwave interactions with the human breast," *IEEE Trans. Biomed. Eng.*, vol. 55, pp. 2792–2800, Dec. 2008.

[24] M. Lazebnik, D. Popovic, L. McCartney, C. B.Watkins, M. J. Lindstrom, J. Harter, S. Sewall, T. Ogilvie, A. Magliocco, T. M. Breslin, W. Temple, D. Mew, J. H. Booske, M. Okoniewski, and S. C. Hagness, "A large-scale study of the ultrawideband microwave dielectric properties of normal, benign and malignant breast tissues obtained from cancer surgeries," *Phys. Med. Biol.*, vol. 52, pp. 6093–6115, 2007.

[25] O. Levy and D. Stroud, "Maxwell Garnett theory for mixtures of anisotropic inclusions: Application to conducting polymers," *Physical Review B*, vol. 56, no. 13, pp. 8035–8046, 1997.

[26] Y. Chen, E. Gunawan, K. S. Low, S.-C. Wang, Y. Kim, and C. B. Soh, "Pulse design for time reversal method as applied to ultrawideband microwave breast cancer detection: A two-dimensional analysis," *IEEE Trans. Antennas Propag.*, vol. 55, no. 1, pp. 194–204, 2007.

[27] W. D. Burside and K. W. Burgener, "High frequency scattering by thin lossless dielectric slab," *IEEE Trans. Antennas Propag.*, vol. AP-31, no. 1, pp. 104–110, 1983.

[28] E. W. Weisstein, "Least squares fitting - Exponential," *MathWorld - A Wolfram Web Resource*, http://mathworld.wolfram.com/LeastSquaresFittingExponential.html.

[29] S. M. Kay, *Fundamentals of Statistical Signal Processing: Estimation Theory*, Prentice-Hall, New Jersey, 1993.

[30] S. Bianco, *Carbon Nanotubes - From Research to Applications*, InTech, 2011.

Figure Captions

- Fig. 1: A schematic illustration of CMI for optimal targeted therapies from the touchable communication channel estimation and waveform design perspective.
- Fig. 2: CMI system setting for estimation of drug nanoparticle accumulation in the tumor. Each antenna element has a different distance of separation from the tumor in order to estimate the drug accumulation in the tumor through the SNR-sensitive information-theoretic-criteria-based signal processing algorithm.
- Fig. 3: (a) Dielectric constant and (b) conductivity of tumor mixed with various volume fractions of drug molecules.
- Fig. 4: Relationships between the normalized SNR and the normalized volume fraction by applying the exact formulation in Section II-C and the approximation in (22), respectively.
- Fig. 5: Relationships between the estimated rank of $\Delta\mathbf{\Psi}_z$ in (20) and the SNR of the differential signal for two information-theoretic criteria.
- Fig. 6: 10 pilot channel impulse responses measured at the antenna array. Also shown are the exact mean response with $\ln \mu_V = \ln 0.2$ and $\zeta = 1.5$ and the estimated mean response with $\ln \hat{\mu}_V = \ln 0.204$ and $\hat{\zeta} = 1.5035$. The estimated standard deviation is $\hat{\sigma}_V = 0.1924$, which is very close to the exact value of $\sigma_V = 0.2$.
- Fig. 7: Relationships between $P_{\rm ISI}$, $P_{\rm NFD}$, and $T_{\rm burst}$ for various elimination rates.
- Fig. 8: (a) Pareto frontiers of $(P_{\rm ISI}, P_{\rm NFD})$ for various elimination rates, and the zoomed-in plots of (a) for (b) $\zeta = 1.3$ day^{-1}, (c) $\zeta = 1.5$ day^{-1}, and (d) $\zeta = 1.7$ day^{-1}.
- Fig. 9: Relationships between BER and $T_{\rm burst}$ for various elimination rates.

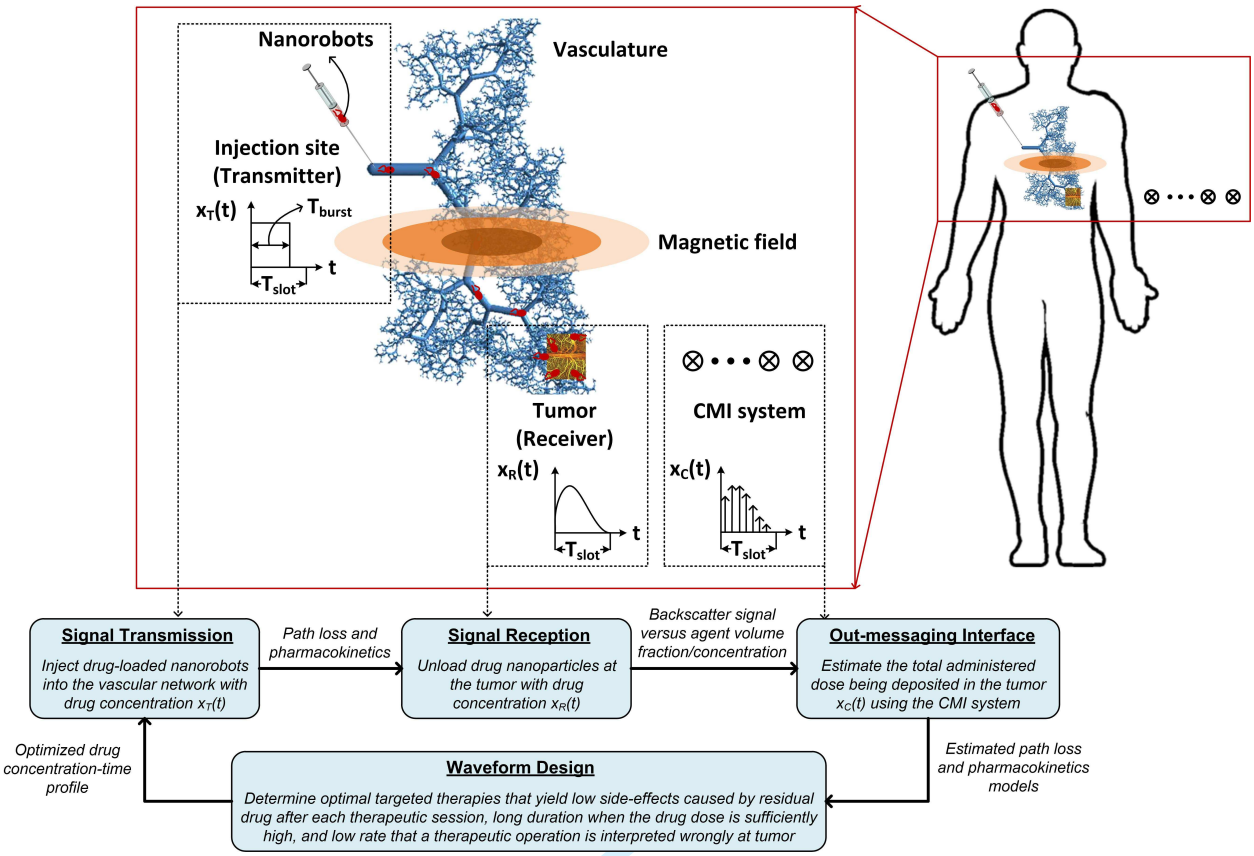

Fig. 1. A schematic illustration of CMI for optimal targeted therapies from the touchable communication channel estimation and waveform design perspective.

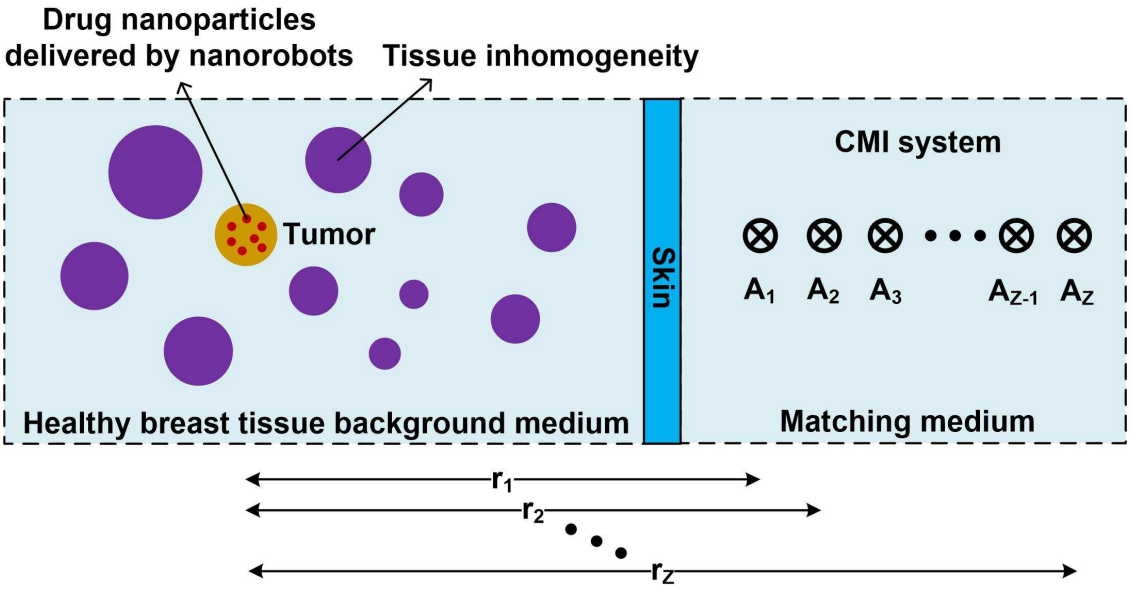

Fig. 2. CMI system setting for estimation of drug nanoparticle accumulation in the tumor. Each antenna element has a different distance of separation from the tumor in order to estimate the drug accumulation in the tumor through the SNR-sensitive information-theoretic-criteria-based signal processing algorithm.

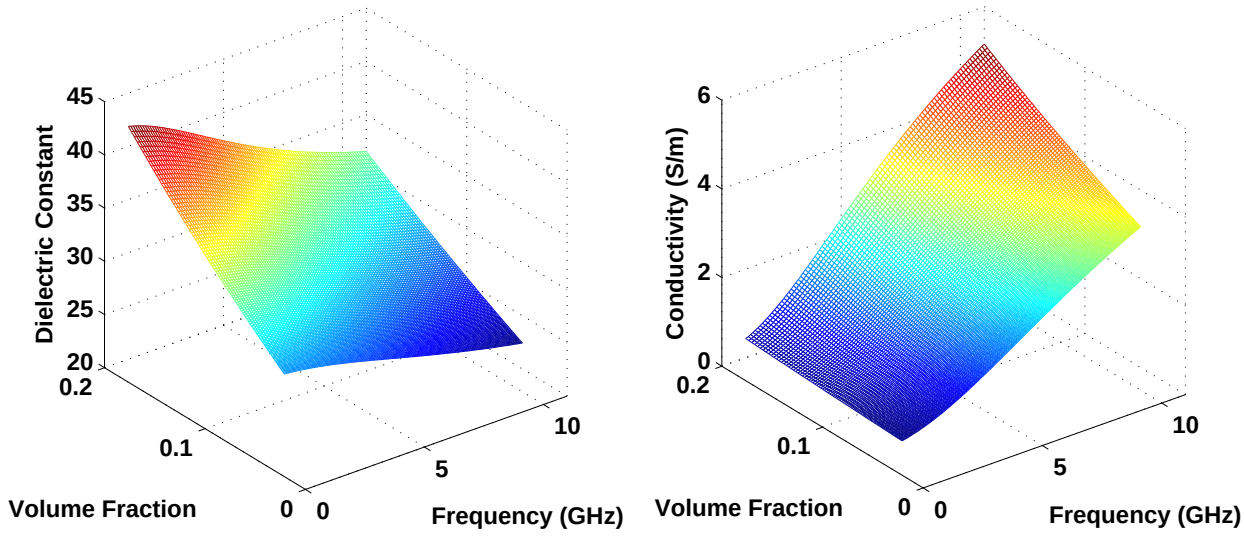

Fig. 3. (a) Dielectric constant and (b) conductivity of tumor mixed with various volume fractions of drug molecules.

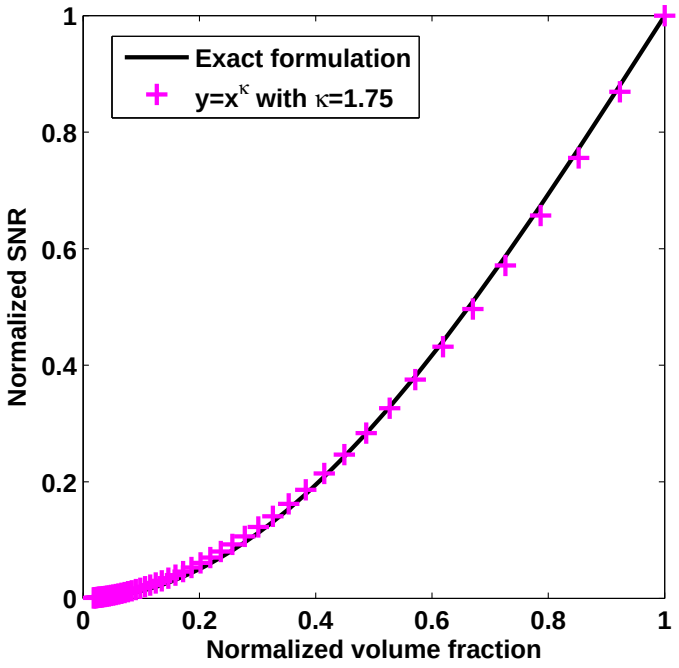

Fig. 4. Relationships between the normalized SNR and the normalized volume fraction by applying the exact formulation in Section II-C and the approximation in (22), respectively.

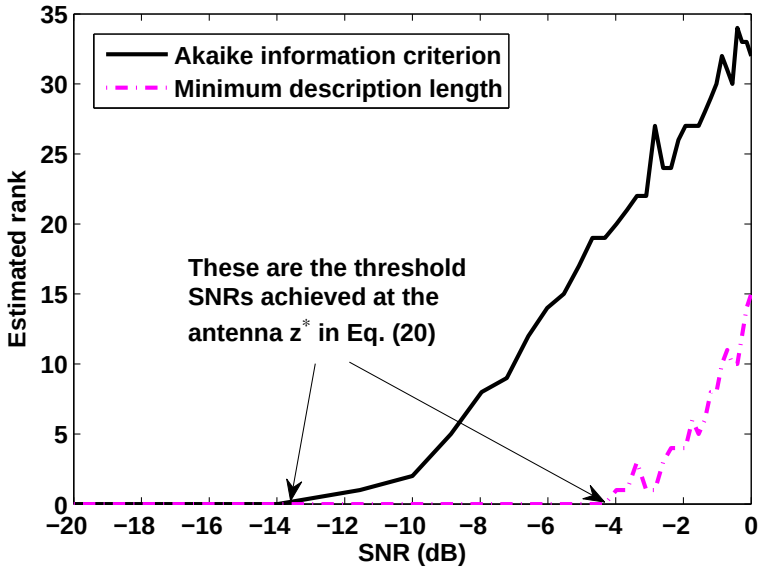

Fig. 5. Relationships between the estimated rank of $\Delta\Psi_z$ in (20) and the SNR of the differential signal for two information-theoretic criteria.

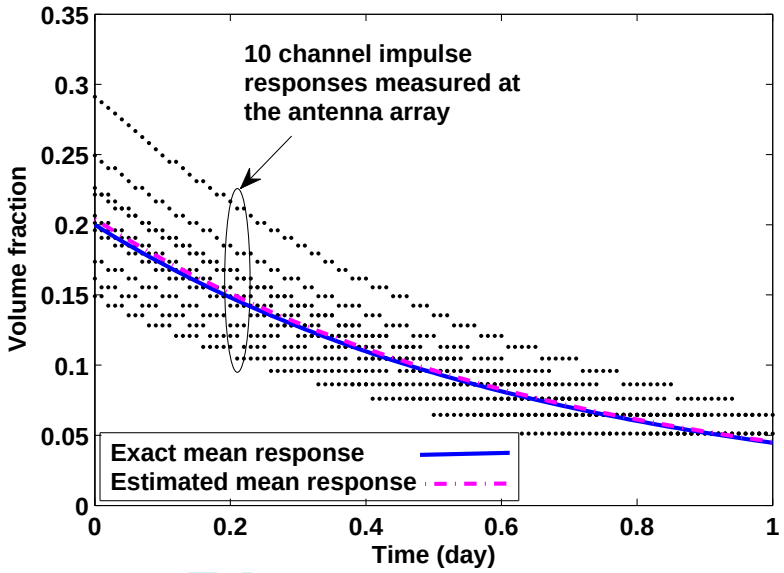

Fig. 6. 10 pilot channel impulse responses measured at the antenna array. Also shown are the exact mean response with $\ln \mu_V = \ln 0.2$ and $\zeta = 1.5$ and the estimated mean response with $\ln \hat{\mu}_V = \ln 0.204$ and $\hat{\zeta} = 1.5035$. The estimated standard deviation is $\hat{\sigma}_V = 0.1924$, which is very close to the exact value of $\sigma_V = 0.2$.

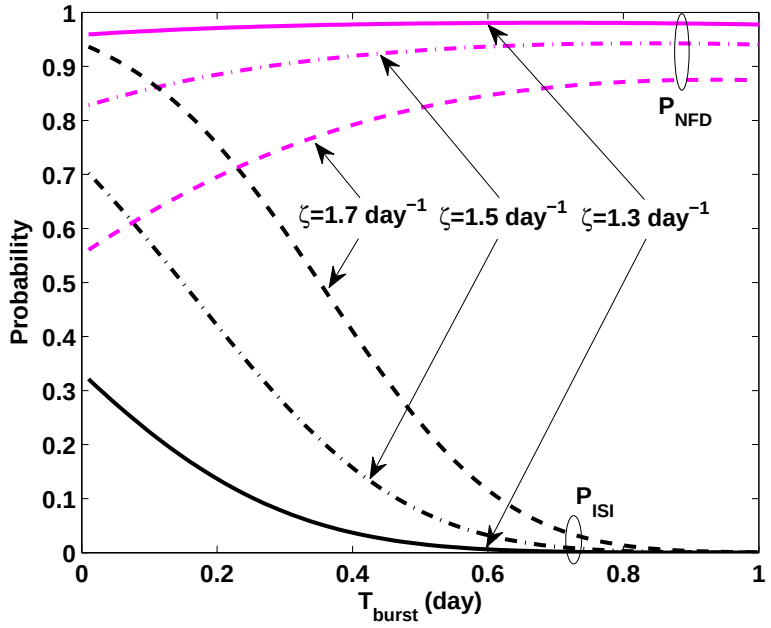

Fig. 7. Relationships between P_{ISI}, P_{NFD}, and T_{burst} for various elimination rates.

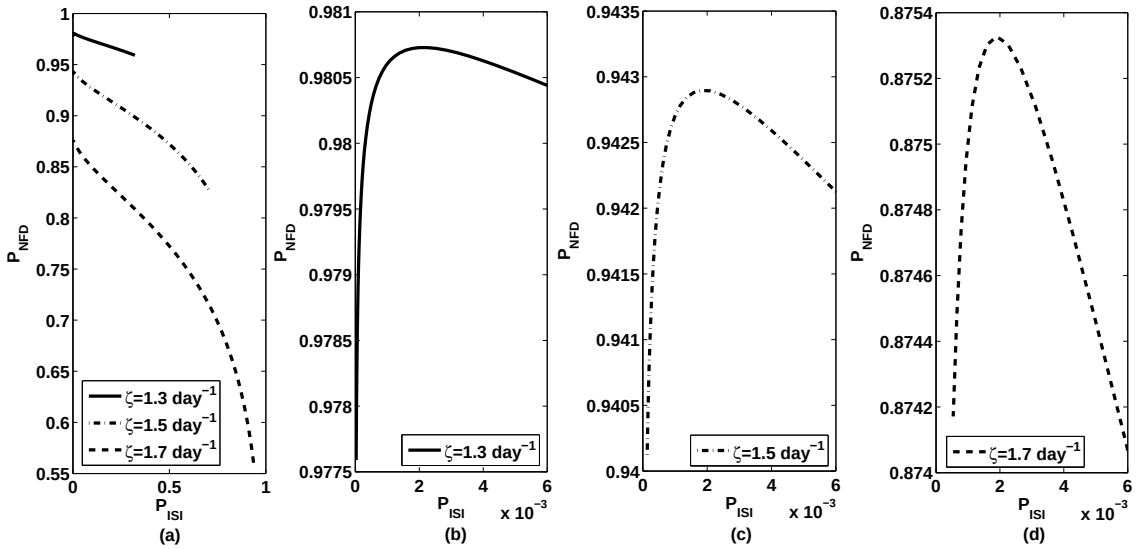

Fig. 8. (a) Pareto frontiers of $(P_{\mathrm{ISI}}, P_{\mathrm{NFD}})$ for various elimination rates, and the zoomed-in plots of (a) for (b) $\zeta = 1.3\ \mathrm{day}^{-1}$, (c) $\zeta = 1.5\ \mathrm{day}^{-1}$, and (d) $\zeta = 1.7\ \mathrm{day}^{-1}$.

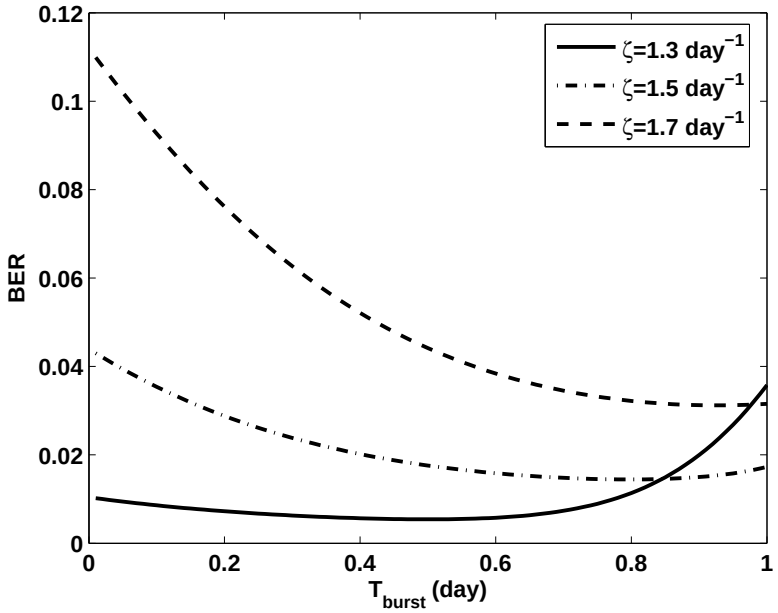

Fig. 9. Relationships between BER and T_{burst} for various elimination rates.

Modeling Contrast-imaging-assisted Optimal Targeted Drug Delivery: A Touchable Communication Channel Estimation and Waveform Design Perspective

Yifan Chen, Yu Zhou, Ross Murch, and Panagiotis Kosmas

***Abstract*—To maximize the effect of treatment and minimize adverse effects on patients, we propose to optimize nanorobots-assisted targeted drug delivery (TDD) for locoregional treatment of tumor from the perspective of touchable communication channel estimation and waveform design. The drug particles are information molecules; the loading/injection and unloading of the drug correspond to the transmitting and receiving processes; the concentration-time profile of drug particles administered corresponds to the signalling pulse. Given this analogy, we first propose to use contrast-enhanced microwave imaging (CMI) as a pretherapeutic evaluation technique to determine the pharmacokinetic model of nanorobots-assisted TDD. The CMI system applies an information-theoretic-criteria-based algorithm to estimate drug accumulation in tumor, which is analogous to the estimation of channel impulse response in the communication context. Subsequently, we present three strategies for optimal targeted therapies from the communication waveform design perspective, which are based on minimization of residual drug molecules at the end of each therapeutic session (i.e., inter-symbol interference), maximization of duration when the drug intensity is above a prespecified threshold during each therapeutic session (i.e., non-fade duration), and minimization of average rate that a therapeutic operation is not received correctly at tumor [i.e., bit error rate (BER)]. Finally, numerical examples are applied to demonstrate the effectiveness of the proposed analytical framework.**

***Index Terms*—Targeted drug delivery, contrast-enhanced microwave imaging, optimal targeted therapies, touchable communication channel estimation and waveform design**

I. Introduction

Nanoparticle-mediated targeted drug delivery (TDD) aims at enhancing locoregional therapies for cancer treatment [1]. These nanoparticles are loaded with drugs and targeted to specific parts of the body where there is solely diseased tissue, thereby avoiding interaction with healthy tissue. The main constraints of the nanocarriers currently administered are the reliance on systemic circulation resulting in only $\sim 2\%$ of the total administered dose being deposited in the tumor, the lack of a propelling force to penetrate the tumor beyond the diffusion limit, and the absence of a sensory-based displacement capability to target the hypoxic zones [2]. Harnessing swarms of magneto-aerotactic bacteria such as the *Magnetococcus marinus* strain MC-1 for delivering drug-containing nanoliposomes to the disease site can significantly improve the therapeutic index of various nanocarriers in tumor regions as demonstrated in [2]. It is crucial to obtain the appropriate concentration-time profile of the therapeutic agent to be injected with respect to the developmental stage of the tumor in order to maximize the effect of treatment and to minimize adverse effects on patients [3].

Molecular communication models can be applied to describe the TDD process [4]–[10]. In molecular communication, an engineered miniature transmitter emits molecules, which propagate and are eventually received by a miniature receiver. The information may be encoded in either the timing or the concentration of molecules. The reception process often involves a chemical reaction between molecules (ligand) and compliant receptors present on the receiver surface. Under this framework, the transmitting process for a TDD system is the drug injection, the receiving process is the drug delivery at a specific target (e.g., tumor), and the channel is realized by the transport of drug particles in the blood stream. The signal is the concentration-time profile of the therapeutic agent, which should be successfully received by the tumor to decrease its size.

This analogy enables the analysis and design of TDD using classical communication tools [4]–[10]. By applying the queuing theory to model receptor saturation, thus treating it as a congestion problem in communication networks, the optimal drug release rate was estimated in [9] to guarantee that the desired fraction of receptors bound to drug molecules without drug overloading. By modeling the pharmacokinetics of TDD systems through the abstraction of molecular communication, including the particle advection, diffusion, absorption, reaction, and adhesion as well as the impact of cardiovascular diseases, the optimal drug injection rate was obtained in [7] to achieve a desired drug delivery rate. In [3], optimal control techniques were applied to find the appropriate treatment and drug dose to decrease the tumor size while minimizing total drug administered for antiangiogenic therapy,

Y. Chen is with the Faculty of Science and Engineering and the Faculty of Computing and Mathematical Sciences, the University of Waikato, Hamilton, New Zealand (e-mail: yifanc@waikato.ac.nz). He is also with the Department of Electrical and Electronic Engineering, Southern University of Science and Technology, Shenzhen, China (e-mail: chen.yf@sustc.edu.cn).

Y. Zhou is with the Department of Electrical and Electronic Engineering, Southern University of Science and Technology, Shenzhen, China. He is also with the Department of Electronic and Computer Engineering, Hong Kong University of Science and Technology, Hong Kong, China.

R. Murch is with the Department of Electronic and Computer Engineering, Hong Kong University of Science and Technology, Hong Kong, China.

P. Kosmas is with the Department of Informatics, King's College London, London, UK.

chemotherapy, and radiotherapy. Finally, optimal shape of the antibody molecular structure was determined in [6] by applying the antibody-mediated TDD system transport and antigen-binding kinetics, taking into account the geometry of the antibody molecule, the electrochemical structure of the antibody-antigen complex, and the physiology of the patient. Nevertheless, the existing works do not discuss how to obtain information of the vascular, extracellular, and ligand-binding channels, which is necessary in order to apply the proposed TDD strategies in real-life applications. Furthermore, none of the works has designed the drug concentration-time profile from the perspective of communication waveform optimization, where the transmission is organized in bursts of drug molecules (i.e., pulses denoting information bits).

The current contribution addresses the aforementioned problems by taking the following approaches. Firstly, interfaces to connect the small-scale *in vivo* environment and the large-scale external environment could be implemented under the paradigm of touchable communication as proposed in [8], [11]. The term "touchable" means that the entire communication process can be controlled and tracked *via* interfaces. Specifically, the in-messaging interfaces convert conventional electronic, magnetic, or optical signals used by the large-scale device into commands to which nanorobots respond by performing subsequent small-scale operations (e.g., through *magnetotaxis* directional control of MC-1 cells [2]), while the out-messaging interfaces convert motion signals generated by nanorobots (e.g., releasing, swimming, and targeting of nanorobots) to externally detectable and interpretable messages [12]. Contrast-enhanced microwave imaging (CMI) can be employed as the out-messaging interface, where the cargo attached to nanorobots is a microwave contrast agent such as carbon nanotubes, which can also serve as a therapeutic agent in cancer treatment [13], [14]. Hence, the CMI technique is proposed for estimation of the TDD pharmacokinetics (equivalently, the impulse response of the touchable communication channel), where two signal-to-noise-ratio (SNR) sensitive information-theoretic criteria [15] are applied to determine the drug disposition in tumor. This estimation step provides exact knowledge about the vascular channel specific to the individual patient and the TDD process undergone, thereby alleviating the issue of wide variety of vasculature across different patients.

Secondly, a novel signal transmission scheme suitable for TDD based on the estimated channel response and the on-off keying scheme is proposed. Three waveform design strategies are then suggested to achieve minimum inter-symbol interference, maximum non-fade duration, and minimum average bit error rate (BER). From the TDD perspective, these criteria yield low side-effects due to residual therapy damaging some healthy tissues after each therapeutic session, long duration when the concentration of drug molecules is sufficiently high, and low average rate that a therapeutic operation is not received correctly at tumor, respectively.

It is worth emphasizing that both the two contributions mentioned above, namely, the CMI for approximation of the TDD pharmacokinetics (channel estimation) and the optimal targeted therapies from the communication perspective (waveform design) have not been covered in our previous works [8], [11], which mainly focus on the general system architecture and channel modeling aspects.

The paper is organized as follows. In Section II, the system and channel models of touchable communication for optimal targeted therapies are investigated. In Section III, the CMI system for estimation of the channel impulse response is presented. In Section IV, the signal transmission process is studied and the waveform optimization strategies are introduced. Finally, Section V provides simulation studies of TDD to demonstrate the principles of the analytical framework, with conclusions drawn in Section VI.

II. Touchable Communication Model of Optimal TDD

The touchable communication model of TDD using drug-loaded nanorobots is illustrated in Fig. 1. The information molecules are therapeutic agents. The binding of drug particles to a swarm of nanorobots such as magneto-aerotactic bacteria and the injection of the swarm into the vascular network at a predefined site are the transmitting process. The transmitted signal $x_{\mathrm{T}}(t)$ is the amount of injected nanoparticles. An external macro-unit generates a magnetic field; the nanorobots sense this field and move towards its gradient *via* magnetotaxis. The propagation process is the touchable communication channel. When the nanorobots reach the tumor, the drug particles will be removed from the vehicles and get assimilated into the targeted issue allowing them to perform healing actions. The unloading operation corresponds to the receiving process. The received signal $x_{\mathrm{R}}(t)$ is the number of nanoparticles successfully discharged at the tumor.

A. Signal Transmission Model

The amount of administered therapeutic agent must be carefully chosen to destroy the tumor, while causing minimal injuries to healthy tissues due to leakage of drug molecules to the systemic flow. To address this issue, optimal control theories have been applied for antiangiogenic therapy, chemotherapy, or radiotherapy [16], [17]. The adaptation of these conventional therapies to the case of magnetically controlled drug-loaded nanoparticles was presented in [3]. Given the specific tumor growth model (e.g., the classical Hahnfeldt's model [18] and its extension [3], [16]), the issue is to find an optimal control input u to decrease the tumor size while minimizing total drug administered. A maximum drug intake $u_{\max}$ has to be enforced. Furthermore, a continuous administration of therapeutic agent has to be realized [3].

From the communication perspective, the transmission process associated with the aforementioned drug administration can be arranged using an on-off scheme consisting of multiple time slots. The period of each slot is T_{slot} as illustrated in Fig. 1, which corresponds to the communication symbol duration. A bit '0' is denoted by the absence of molecule within a time slot. On the other hand, a bit '1' is denoted by a burst of molecules $x_{\mathrm{T}}(t)$ over a short period equal to T_{burst} where $T_{\mathrm{burst}} \leq T_{\mathrm{slot}}$. For normalized $x_{\mathrm{T}}(t)$ satisfying $\int_0^{T_{\mathrm{slot}}} x_{\mathrm{T}}(t)dt = \int_0^{T_{\mathrm{burst}}} x_{\mathrm{T}}(t)dt = 1$, the optimal

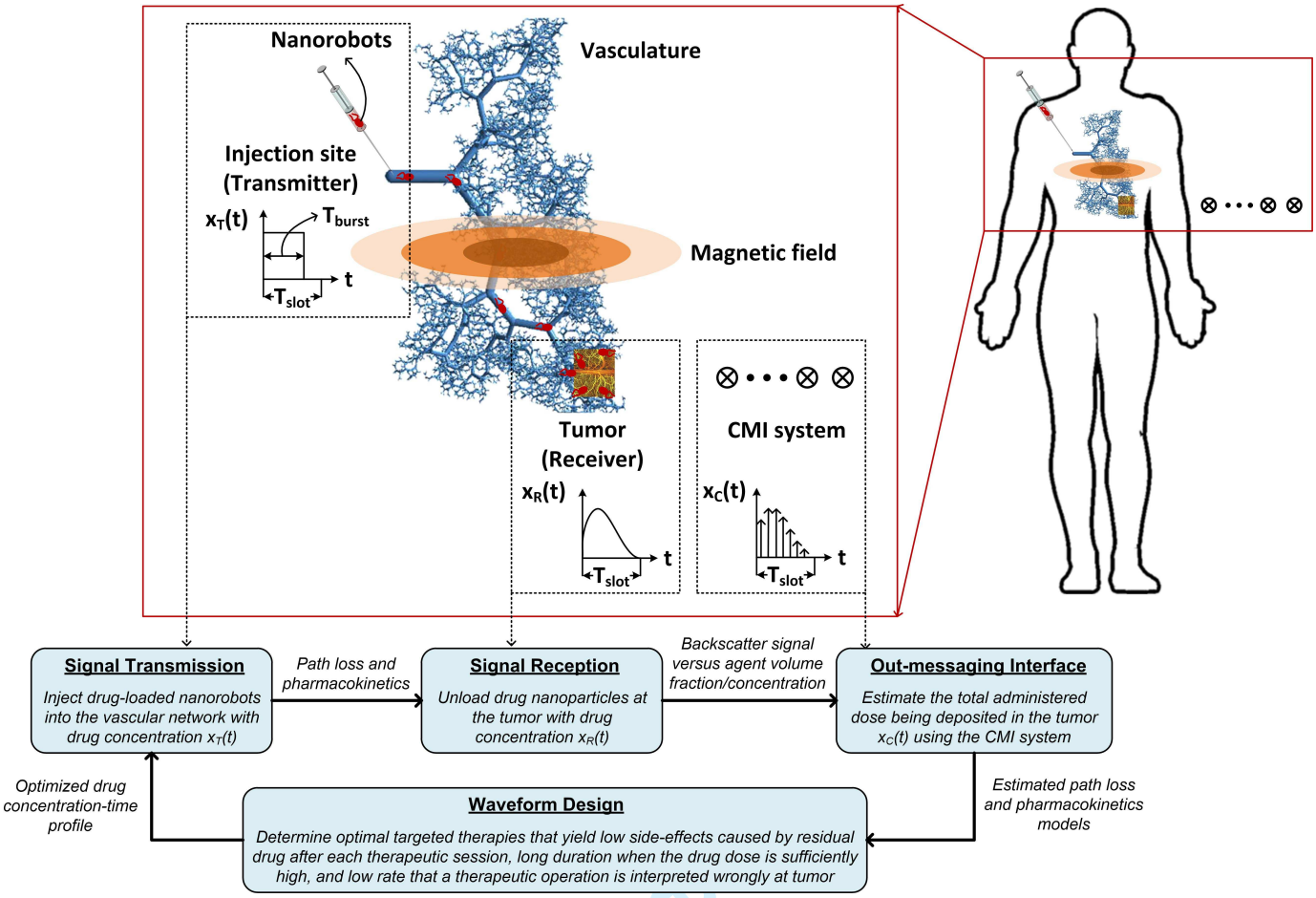

Fig. 1. A schematic illustration of CMI for optimal targeted therapies from the touchable communication channel estimation and waveform design perspective.

control input u_i emulated by the i^{th} cluster of continuous emissions of drug molecules is:

$$u_i = \int_0^{u_i T_{\text{slot}}} x_{\text{T}}(t)dt = u_i \int_0^{T_{\text{burst}}} x_{\text{T}}(t)dt. \quad (1)$$

As such, u_i also denotes the number of bits over the i^{th} cluster of continuous emissions. Furthermore, the drug intake has to be saturated to an upper limit such that $u_i \leq u_{\max}$. This on-off scheme represents both a clinically relevant drug administration process and a useful analytical framework for optimal direct targeting therapy under the rubric of information transmission, which allows for application of the classical communication performance measures such as inter-symbol interference, non-fade duration, and BER to system design as to be made clear in the following sections.

B. Signal Reception Model

The signal reception process is characterized by the pharmacokinetics model, which describes how the therapeutic agent is absorbed, distributed, and eliminated by the body and is commonly modeled through the agent concentration in the sampled fluid (e.g., plasma or blood) at the host, $x_{\text{R}}(t)$. A compartmental modeling analysis has been widely employed. For example, the compartment models best-fit the concentration-time profiles of plasma temozolomide, which is an agent effective for treating gliomas, in cerebrospinal fluid, normal brain, and brain tumor tissues in a rat orthotopic brain tumor model [19]. The one-compartment model was applied in modeling the biodistribution of drug-loaded magnetic nanoparticles for the liver cancer [3], which is similar to the situation of nanorobots-assisted TDD considered here. Under this circumstance, the input is equal to the dose at the initial time point 0 and becomes 0 thereafter. The concentration at time 0 corresponds to the dose divided by the volume of the tumor, and the concentration decreases with time in an exponential manner.

Hence, the following agent concentration expression is derived:

$$x_{\text{R}}(t) = \int_{\tau} \rho x_{\text{T}}(\tau) \exp\left[-\zeta(t-\tau)\right] d\tau, \quad (2)$$

where ρ is the path loss from the injection site to the tumor and ζ is the drug clearance rate. The path loss consists of three different components for touchable communication [8]: diffusion, branching, and resorption. Each loss component reduces certain amount of nanorobots, and the overall attenuation is obtained as the multiplication of these components.

The diffusion occurs in the systemic flow due to the random Brownian motions of nanorobots; the branching occurs at the entrance of the intended daughter branch when the vessels are too slender to be imaged. The resorption quantifies the effect of biodegradation on the amount of nanorobots consumed. Detailed derivations of the path loss ρ can be found in [8]. As ρ is the multiplicative product of multiple independent random variables, it can be approximated using a lognormal distribution by considering the central limit theorem in the log domain, which is similar to the lognormal shadowing effect in classical wireless communications:

$$f_\rho(\rho) = \frac{1}{\rho\sigma_\rho\sqrt{2\pi}} e^{-\frac{(\ln\rho-\mu_\rho)^2}{2\sigma_\rho^2}}. \tag{3}$$

The two parameters μ_ρ and σ_ρ are, respectively, the mean and standard deviation of $\ln\rho$. In addition, the drug clearance rate describes how fast the drug is filtered out of the blood. The clearance is often modeled as a constant for a specific biological system.

It is worth emphasizing that the model in (2) is concise with a small number of unknown parameters, which is advantageous from the channel estimation perspective but may miss out on some useful details about the vascular network. Thus, it is important for the TDD system designer to achieve a balanced trade-off between channel model accuracy and estimation efficiency.

C. Out-messaging Interface Model

CMI can be employed as the out-messaging interface to estimate the total administered dose being deposited in the tumor. The cargo attached to nanorobots is a microwave contrast agent such as carbon nanotubes, ferroelectric nanoparticles, or magnetic nanoparticles, which can also be employed as a therapeutic agent [13], [15], [20]–[22]. The contrast agent alters the dielectric property of the targeted tissue. Differential microwave imaging can then be applied to monitor backscatter signature over time, which images temporal variation in tissue anomaly and provides information on the therapeutic index of various nanoparticles in tumor. For illustration, breast cancer imaging is considered in the current work, where a schematic diagram of the CMI system is shown in Fig. 2. The same figure also shows a tumorous lesion buried in a cluttered background medium generated by tissue inhomogeneities.

Firstly, a single-pole Cole-Cole model is employed to describe the frequency dependence of the complex permittivity, $\varepsilon_{\text{breast}}$, of healthy breast tissue background medium over the band of interest (100 MHz to 20 GHz) [23]:

$$\varepsilon_{\text{breast}}(\omega) = F_1 + \frac{F_2}{1+(j\omega F_3)^{1-F_4}} + \frac{F_5}{j\omega\varepsilon_0}, \tag{4}$$

where ω is the frequency in radian, ε_0 is the permittivity of free space, and $F_1 \sim F_5$ are fitting parameters. Secondly, in terms of tumor permittivity, $\varepsilon_{\text{tumor}}$, it has been shown that there is a large variation in the dielectric contrast between malignant and healthy breast tissues due to substantial heterogeneity and the contrast ranges from no more than 10% to fivefold [24]. Furthermore, the complex permittivity of tumor penetrated by

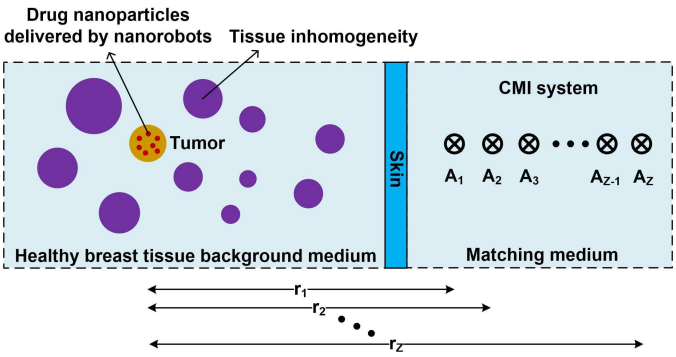

Fig. 2. CMI system setting for estimation of drug nanoparticle accumulation in the tumor. Each antenna element has a different distance of separation from the tumor in order to estimate the drug accumulation in the tumor through the SNR-sensitive information-theoretic-criteria-based signal processing algorithm.

nanorobots and attached with contrast medium nanocomposites can be approximated by applying the classical Maxwell Garnett equation [25]:

$$\tilde{\varepsilon}_{\text{tumor}}(\omega) = \varepsilon_{\text{tumor}}(\omega)\times \frac{[\varepsilon_{\text{agent}}(\omega)+2\varepsilon_{\text{tumor}}(\omega)]+2V_{\text{agent}}[\varepsilon_{\text{agent}}(\omega)-\varepsilon_{\text{tumor}}(\omega)]}{[\varepsilon_{\text{agent}}(\omega)+2\varepsilon_{\text{tumor}}(\omega)]-V_{\text{agent}}[\varepsilon_{\text{agent}}(\omega)-\varepsilon_{\text{tumor}}(\omega)]}, \tag{5}$$

where $\tilde{\varepsilon}_{\text{tumor}}$ is the effective dielectric constant of tumor resulting from the inclusion of a volume fraction V_{agent} of contrast agent nanoparticles with dielectric constant $\varepsilon_{\text{agent}}$.

The next step is to derive the waveforms scattered by tumor. It is assumed that the antennas are immersed in a coupling medium with dielectric property matching the breast permittivity over the entire frequency band [15]. Consider a tumor oriented parallel to multiple spatially diverse monostatic antenna elements (i.e., the transmitter and receiver are collocated), $A_1, A_2, \cdots, A_Z$, generating equal electric current line sources, $i(t)$. The distances between the antennas and the tumor are $r_1 < r_2 < \cdots < r_Z$ as shown in Fig. 2. In the absence of a skin layer, the frequency-domain expression of the backscatter field at A_z $(z = 1, 2, \cdots, Z)$ is [26]:

$$I(\omega)\left[\frac{\omega\mu_0}{4}\sum_{\nu=-\infty}^{+\infty}\mathcal{K}_\nu(\omega)\mathcal{H}_\nu^{(2)}(k_{\text{breast}}r_z)\right], \tag{6}$$

where

$$\mathcal{K}_\nu(\omega) = \left\{\mathcal{J}_\nu'\left(\frac{k_{\text{breast}}d_{\text{tumor}}}{2}\right)\mathcal{J}_\nu\left(\frac{\tilde{k}_{\text{tumor}}d_{\text{tumor}}}{2}\right) - \sqrt{\frac{\tilde{\varepsilon}_{\text{tumor}}(\omega)}{\varepsilon_{\text{breast}}(\omega)}}\mathcal{J}_\nu\left(\frac{k_{\text{breast}}d_{\text{tumor}}}{2}\right)\mathcal{J}_\nu'\left(\frac{\tilde{k}_{\text{tumor}}d_{\text{tumor}}}{2}\right)\right\} \Big/ \left\{\sqrt{\frac{\tilde{\varepsilon}_{\text{tumor}}(\omega)}{\varepsilon_{\text{breast}}(\omega)}}\mathcal{H}_\nu^{(2)}\left(\frac{k_{\text{breast}}d_{\text{tumor}}}{2}\right)\mathcal{J}_\nu'\left(\frac{\tilde{k}_{\text{tumor}}d_{\text{tumor}}}{2}\right) - \mathcal{H}_\nu^{(2)'}\left(\frac{k_{\text{breast}}d_{\text{tumor}}}{2}\right)\mathcal{J}_\nu\left(\frac{\tilde{k}_{\text{tumor}}d_{\text{tumor}}}{2}\right)\right\}. \tag{7}$$

The term μ_0 is the permeability of free space, I is the frequency-domain representation of the current source, $\mathcal{H}_\nu^{(2)}$ is the ν^{th}-order Hankel function of the second kind, and $\mathcal{J}_\nu$ is the ν^{th}-order Bessel function. The prime $(')$ denotes a derivative with respect to the argument of the function, d_{tumor} is the diameter of the tumor, and k_{breast} and $\tilde{k}_{\text{tumor}}$ are the wavenumbers for the tissue background medium and the tumor mixed with nanoparticles, respectively. The propagation effects of a plane wave in the skin for the round-trip distances traveled are separately accounted for. To include a skin layer with relative dielectric constant $\varepsilon_{\text{skin}}$ and conductivity σ_{skin}, the slab model is applied where the skin response is given by [27]:

$$H_{\text{skin}}(\omega) = \left\{ \frac{\left[1 - R_{\text{skin}}^2(\omega)\right] e^{-j[k_{\text{skin}}(\omega) - k_{\text{breast}}(\omega)]\xi_{\text{skin}}}}{1 - R_{\text{skin}}^2(\omega) e^{-j2k_{\text{skin}}(\omega)\xi_{\text{skin}}}} \right\}^2. \tag{8}$$

The term R_{skin} is the Fresnel reflection coefficient of single reflection exterior to the skin layer, ξ_{skin} is the thickness of the skin, and k_{skin} is the wavenumber for skin. Subsequently, time-domain backscatter signals are obtained from (6) and (8) by performing an inverse Fourier transform for a set of frequencies spanning the band of interest:

$$\begin{aligned} & o_{\text{tumor}}(t) \\ &= \mathbb{F}^{-1}\left\{ I(\omega) \left[\frac{\omega\mu_0}{4} \sum_{\nu=-\infty}^{+\infty} \mathcal{K}_\nu(\omega) \mathcal{H}_\nu^{(2)}\left(k_{\text{breast}} r_z\right) \right] H_{\text{skin}}(\omega) \right\} \\ &= \mathbb{F}^{-1}\left\{ I(\omega) H_{\text{tumor}}(\omega) \right\}, \end{aligned} \tag{9}$$

where H_{tumor} is the frequency-domain channel response due to tumor and $\mathbb{F}^{-1}$ denotes inverse Fourier transform. The backscatter signal due to tissue inhomogeneity can be obtained in a similar manner by replacing the tumor dielectric properties with the tissue heterogeneity dielectric constant and conductivity.

Finally, it is important to determine the relationship between the agent concentration at the host, x_{R} in (2), and the volume fraction V_{agent} in (5). Let D_{agent} and M_{agent} denote, respectively, the density and mass of agent nanoparticles. Let $\mathbb{V}_{\text{tumor}}$ denote the tumor volume. It can be easily shown that M_{agent}, which is proportional to x_{R}, is given by $M_{\text{agent}} = D_{\text{agent}} \frac{\mathbb{V}_{\text{tumor}} V_{\text{agent}}}{1 - V_{\text{agent}}}$. Consequently, in the real-life situation of $V_{\text{agent}} \ll 1$, x_{R} is proportional to V_{agent}, which in turn determines the effective dielectric constant of tumor $\tilde{\varepsilon}_{\text{tumor}}$ and the received backscatter signal $o_{\text{tumor}}(t)$ in (9). Hence, by monitoring the variation of $o_{\text{tumor}}(t)$ over time due to drug deposition and elimination, the touchable communication channel represented by the input-output relationship in (2) can be estimated as to be discussed in the following section.

III. Estimation of TDD Pharmacokinetic Model

A. Estimation of Contrast Agent Concentration

The information-theoretic-criteria-based tumor detection algorithm in [15] is revisited here in the current problem setting. Let $i_z(t)$ and $o_z(t)$ denote, respectively, the continuous-time excitation current and the overall signal received by A_z. Note that o_z includes both the tumor response $o_{\text{tumor},z}$ given by (9) and the tissue inhomogeneity response at A_z. In the frequency domain, the following general relationship can be obtained:

$$o_z(t) = \int_0^{T_{\text{sc},z}} h_z(\tau) i_z(t-\tau) d\tau + w_z(t), \tag{10}$$

where h_z is the continuous channel response, w_z is the additive white Gaussian noise, and $T_{\text{sc},z}$ is the length of the scattering channel. Sampling the received signal at rate f_0 and defining the following notations $o_z(m) = o_z(m/f_0)$, $i_z(m) = i_z(m/f_0)$, and $w_z(m) = w_z(m/f_0)$, the following discrete representation is obtained:

$$o_z(m) = \sum_{l=0}^{L_z - l} h_z(l) i_z(m-l) + w_z(m), \tag{11}$$

where $h_z(l)$ denotes the discrete channel response of $h_z(l/f_0)$ and L_z denotes the order of the discrete channel. Eq. (11) can be rewritten in the matrix form as

$$\mathbf{o}_z = \mathbf{H}_z \mathbf{i}_z + \mathbf{w}_z, \tag{12}$$

where

$$\mathbf{o}_z = \left[o_z((n-1)(L_z + M_z - 1) + 1) \ \cdots \ o_z(n(L_z + M_z - 1)) \right]^T, \tag{13}$$

$$\mathbf{H}_z = \begin{bmatrix} & & & h_z(0) \\ & & h_z(0) & h_z(1) \\ & \iddots & \vdots & \vdots \\ h_z(0) & h_z(1) & \cdots & h_z(M_z - 1) \\ h_z(1) & h_z(2) & \cdots & h_z(M_z) \\ \vdots & \vdots & \iddots & \\ h_z(L_z - 2) & h_z(L_z - 1) & & \\ h_z(L_z - 1) & & & \end{bmatrix}, \tag{14}$$

$$\mathbf{i}_z = \left[i_z(nM_z) \ \cdots \ i_z((n-1)M_z + 1) \right]^T, \tag{15}$$

$$\mathbf{w}_z = \left[w_z((n-1)(L_z + M_z - 1) + 1) \ \cdots \ w_z(n(L_z + M_z - 1)) \right]^T. \tag{16}$$

In (13)-(16), $n = 1, 2, \cdots, N$ is the index of each observation, M_z is the signal length, and $\mathbf{o}_z$, $\mathbf{H}_z$, $\mathbf{i}_z$, and $\mathbf{w}_z$ are the observation vector, the channel matrix, the source signal vector, and the noise vector, respectively. The symbol $(^T)$ denotes matrix transpose.

Suppose that the delay introduced by a tumor is ℓ_z/f_0 $(0 < \ell_z \leq L_z - 1)$. the early-time responses caused by healthy tissue heterogeneities that yield time-of-arrival less than ℓ_z/f_0 can be distinguished from the late-time responses due to the cancer itself, healthy tissue inhomogeneities, as well as mutual interference between the cancer and other scattering centers with time-of-arrival no less than ℓ_z/f_0. Drug deposition in the cancer will distort the scattering channel responses caused by changes in the tumor dielectric properties, and only the late responses will be influenced. The new channel matrix after infusion of contrast agent is given by

$$\tilde{\mathbf{H}}_z = \mathbf{H}_z + \Delta\mathbf{H}_z, \tag{17}$$

where the $(i,j)^{\text{th}}$ $(i = 1,2,\cdots,L_z+M_z-1; j = 1,2,\cdots,M_z)$ entry of the perturbation matrix $\Delta\mathbf{H}_z$ is expressed as

$$\Delta\mathbf{H}_z[i,j] = \begin{cases} 0; & \text{if } \mathbf{H}_z[i,j] = 0 \\ 0; & \text{if } \mathbf{H}_z[i,j] = h_z(l) \text{ and } l < \ell_z \\ \Delta h_z(l); & \text{if } \mathbf{H}_z[i,j] = h_z(l) \text{ and } l \geq \ell_z \end{cases} \tag{18}$$

In (18), $\Delta h_z(l)$ is a nonzero term summarizing the overall perturbation effect introduced to the l^{th} tap of the scattering channel.

CMI relies upon the difference between the backscatter responses with and without contrast medium delivered to the cancer, viz.,

$$\begin{aligned} \Delta\mathbf{o}_z &= \tilde{\mathbf{o}}_z - \mathbf{o}_z \\ &= \tilde{\mathbf{H}}_z\mathbf{i}_z + \tilde{\mathbf{w}}_z - (\mathbf{H}_z\mathbf{i}_z + \mathbf{w}_z) \\ &= \Delta\mathbf{H}_z\mathbf{i}_z + \Delta\mathbf{w}_z, \end{aligned} \tag{19}$$

where $\tilde{\mathbf{w}}_z$ is the noise associated with the post-contrast scattered signals. Note that $\Delta\mathbf{w}_z = \tilde{\mathbf{w}}_z - \mathbf{w}_z$ is also an additive white Gaussian noise. A close examination of (18) reveals that the first ℓ_z rows of $\Delta\mathbf{H}_z$ $(z = 1,2,\cdots,Z)$ are empty vectors. Apparently, $\text{rank}\,(\Delta\mathbf{H}_z) \leq \min(L_z+M_z-1-\ell_z, M_z) = M_z$ by noting that $L_z \geq \ell_z + 1$. If we assume that the matrix $\Delta\mathbf{H}_z$ is of full column rank and the covariance matrix $\mathbf{I}_z = \mathbb{E}\{\mathbf{i}_z(t)\mathbf{i}_z^\dagger(t)\}$, where $\mathbb{E}$ denotes expectation, is nonsingular for all z, the rank of the covariance matrix $\Delta\mathbf{\Psi}_z = \Delta\mathbf{H}_z\mathbf{I}_z\Delta\mathbf{H}_z^\dagger$ is M_z. The information-theoretic criteria such as the Akaike information criterion or the minimum description length [15] can thus be applied to estimate the signal-to-noise ratio (SNR) $\eta_z = \|\Delta\mathbf{H}_z\mathbf{i}_z\|^2 / \mathbb{E}\left\{\|\Delta\mathbf{w}_z\|^2\right\}$.

Essentially, when an antenna A_z is far away from the tumor and η_z is very low, the received differential signal $\Delta\mathbf{o}_z$ only consists of the noise samples. Therefore, the estimated rank of $\triangle\mathbf{\Psi}_z$ *via* the information-theoretic criteria should be zero. On the contrary, if A_z is near the tumor and η_z is sufficiently large, there will be residual non-zero entries in $\Delta\mathbf{H}_z$. Therefore, the number of signals will be larger than zero. Subsequently, at any observation time t, we identify the antenna index $z^*(t)$ such that:

$$z^*(t) = \max\left\{z(t) \in \{1,2,\cdots,Z\} : \text{rank}\left(\triangle\mathbf{\Psi}_{z(t)}\right) > 0\right\}. \tag{20}$$

The corresponding normalized SNR is obtained as:

$$\begin{aligned} \bar{\eta}_{z^*(t)} &= \frac{r_{z^*(t)}\eta^*}{r_{z^*(0)}\eta^*} \\ &= \frac{r_{z^*(t)}}{r_{z^*(0)}}, \end{aligned} \tag{21}$$

where η^* represents the threshold SNR below which the CMI system is unable to detect the tumor. The two terms $r_{z^*(t)}$ and $r_{z^*(0)}$ are the distances from the tumor to antennas $A_{z^*(t)}$ and $A_{z^*(0)}$, respectively, where time 0 denotes the initial instant when nanorobots have just arrived at the tumor. These two factors compensate for radial spreading resulting in decrease in amplitude of an electromagnetic wave as it expands.

Finally, the normalized SNR $\bar{\eta}_{z^*(t)}$ increases monotonically with the time-varying volume fraction $V_{\text{agent}}(t)$ [see also (5)]. Instead of using the exact but complex relationship between $\bar{\eta}_{z^*(t)}$ and $V_{\text{agent}}(t)$ as presented in the previous section, the following simple yet versatile function is considered:

$$\bar{\eta}_{z^*(t)} = \left[\frac{V_{\text{agent}}(t)}{V_{\text{agent}}(0)}\right]^\kappa [\theta(t) - \theta(t-1)], \tag{22}$$

where $V_{\text{agent}}(0)$ is the volume fraction at the initial time 0 and $\theta(\cdot)$ is the Heaviside step function. For $\kappa \to \infty$, Eq. (22) describes the case that $\bar{\eta}_{z^*(t)}$ is more sensitive to $V_{\text{agent}}(t)$ in the large volume fraction regime. The case when $\bar{\eta}_{z^*(t)}$ varies more significantly with $V_{\text{agent}}(t)$ at low volume fraction is given by $\kappa \to 0$.

As the information-theoretic method was successfully applied to more complicated breast phantoms for tumor detection in [15], it is expected that the methodology would be applicable to a wide variety of breast models for estimation of contrast agent concentration.

B. Estimation of Pharmocokinetic Model

Estimation of the pharmocokinetic model is achieved by sending Q impulses of contrast agent nanoparticle and measuring the corresponding pilot channel responses at the tumor in terms of volume fraction. The volume fraction at the initial time $V_{\text{agent}}(0)$ is proportional to the path loss ρ in (2) in the practical scenario of $V_{\text{agent}}(0) \ll 1$. Therefore, following (2), for the q^{th} $(q = 1,2,\cdots,Q)$ probing impulse, its response in terms of volume fraction can be expressed as:

$$V_{\text{agent},q}(t) = V_{\text{agent},q}(0)e^{-\zeta t} + \text{noise}, \tag{23}$$

where the subscript q denotes the model parameters for the q^{th} impulse. In order to weight the measurement points equally in least squares fitting, the objective is to minimize the function:

$$\sum_{p=1}^{P} V_{\text{agent},q}(t_p)\left[\ln V_{\text{agent},q}(t_p) - \ln V_{\text{agent},q}(0) + \zeta t_p\right]^2 \tag{24}$$

over P measurement times for any q, which yields the following solutions [28]:

$$\begin{aligned} &\ln\hat{V}_{\text{agent},q}(0) = \\ &\sum_{p=1}^{P}\left[t_p^2 V_{\text{agent},q}(t_p)\right]\sum_{p=1}^{P}\left[V_{\text{agent},q}(t_p)\ln V_{\text{agent},q}(t_p)\right] \Big/ \\ &\left\{\sum_{p=1}^{P} V_{\text{agent},q}(t_p)\sum_{p=1}^{P}\left[t_p^2 V_{\text{agent},q}(t_p)\right] - \left[\sum_{p=1}^{P} t_p V_{\text{agent},q}(t_p)\right]^2\right\} \\ &- \sum_{p=1}^{P}\left[t_p V_{\text{agent},q}(t_p)\right]\sum_{p=1}^{P}\left[t_p V_{\text{agent},q}(t_p)\ln V_{\text{agent},q}(t_p)\right] \Big/ \\ &\left\{\sum_{p=1}^{P} V_{\text{agent},q}(t_p)\sum_{p=1}^{P}\left[t_p^2 V_{\text{agent},q}(t_p)\right] - \left[\sum_{p=1}^{P} t_p V_{\text{agent},q}(t_p)\right]^2\right\} \end{aligned} \tag{25}$$

and

$$\hat{\zeta}_q = -\sum_{p=1}^{P} V_{\text{agent},q}(t_p) \sum_{p=1}^{P} \left[t_p V_{\text{agent},q}(t_p) \ln V_{\text{agent},q}(t_p)\right] \Bigg/ \left\{\sum_{p=1}^{P} V_{\text{agent},q}(t_p) \sum_{p=1}^{P} \left[t_p^2 V_{\text{agent},q}(t_p)\right] - \left[\sum_{p=1}^{P} t_p V_{\text{agent},q}(t_p)\right]^2\right\} + \sum_{p=1}^{P} \left[t_p V_{\text{agent},q}(t_p)\right] \sum_{p=1}^{P} \left[V_{\text{agent},q}(t_p) \ln V_{\text{agent},q}(t_p)\right] \Bigg/ \left\{\sum_{p=1}^{P} V_{\text{agent},q}(t_p) \sum_{p=1}^{P} \left[t_p^2 V_{\text{agent},q}(t_p)\right] - \left[\sum_{p=1}^{P} t_p V_{\text{agent},q}(t_p)\right]^2\right\} \tag{26}$$

The symbol $(\hat{\cdot})$ denotes an estimated quantity. Note that as the drug elimination rate is a constant, the final least-squares estimate of ζ is obtained as:

$$\hat{\zeta} = \frac{1}{Q} \sum_{q=1}^{Q} \hat{\zeta}_q. \tag{27}$$

Similar to the path loss ρ, the volume fraction $V_{\text{agent}}(0)$ is also log-normally distributed. For determining the maximum likelihood estimator of the lognormal distribution parameters μ_V and σ_V for $V_{\text{agent}}(0)$, the log-likelihood function is written as:

$$\mathcal{L}_{LN}\left(\mu_V, \sigma_V \middle| \hat{V}_{\text{agent},1}(0), \hat{V}_{\text{agent},2}(0), \cdots, \hat{V}_{\text{agent},Q}(0)\right) = -\sum_{q=1}^{Q} \ln \hat{V}_{\text{agent},q}(0) + \mathcal{L}_N\left(\mu_V, \sigma_V \middle| \ln \hat{V}_{\text{agent},1}(0), \ln \hat{V}_{\text{agent},2}(0), \cdots, \ln \hat{V}_{\text{agent},Q}(0)\right), \tag{28}$$

where $\mathcal{L}_N$ denotes the log-likelihood function of a normal distribution. Since the first term in (28) is constant with regard to μ_V and σ_V, both logarithmic likelihood functions, $\mathcal{L}_{LN}$ and $\mathcal{L}_N$, reach their maximum with the same μ_V and σ_V. Hence, using the formulas for the normal distribution maximum likelihood parameter estimators, for the log-normal distribution it holds that [29]:

$$\hat{\mu}_V = \frac{\sum_{q=1}^{Q} \ln \hat{V}_{\text{agent},q}(0)}{Q} \tag{29}$$

and

$$\hat{\sigma}_V^2 = \frac{\sum_{q=1}^{Q} \left[\ln \hat{V}_{\text{agent},q}(0) - \hat{\mu}_V\right]^2}{Q}. \tag{30}$$

IV. Optimization of Concentration-Time Profile of Injected Drug Molecules

Three waveform design strategies are proposed in this section to achieve minimum inter-symbol interference, maximum non-fade duration, and minimum BER. From the TDD perspective, these criteria yield low side-effects caused by residual drug after each therapeutic session, long duration when the drug dose is sufficiently high, and low rate that a therapeutic operation is interpreted wrongly at tumor, respectively.

For simplicity, we assume that $x_{\text{T}}(t)$ is a boxcar function given by $x_{\text{T}}(t) = \frac{1}{T_{\text{burst}}}\left[\theta(t) - \theta(t - T_{\text{burst}})\right]$. The output signal is computed as:

$$x_{\text{R}}(t) = \begin{cases} \int_0^t \frac{\rho}{T_{\text{burst}}} \exp\left[-\zeta(t-\tau)\right] d\tau, & 0 \le t \le T_{\text{burst}} \\ \int_0^{T_{\text{burst}}} \frac{\rho}{T_{\text{burst}}} \exp\left[-\zeta(t-\tau)\right] d\tau, & t > T_{\text{burst}} \end{cases} = \begin{cases} \frac{\rho[1-\exp(-\zeta t)]}{\zeta T_{\text{burst}}}, & 0 \le t \le T_{\text{burst}} \\ \frac{\rho\{\exp[-\zeta(t-T_{\text{burst}})]-\exp(-\zeta t)\}}{\zeta T_{\text{burst}}}, & t > T_{\text{burst}} \end{cases} \tag{31}$$

Therefore, the probability that $x_{\text{R}}(t)$ at the end of each symbol duration, $t = T_{\text{slot}}$, is no greater than a specified threshold x_{ISI} is derived as:

$$\begin{aligned} P_{\text{ISI}} &= \Pr\left\{x_{\text{R}}(T_{\text{slot}}) \le x_{\text{ISI}}\right\} \\ &= \Pr\left\{\rho \le \frac{\zeta T_{\text{burst}} x_{\text{ISI}}}{\exp\left[-\zeta\left(T_{\text{slot}} - T_{\text{burst}}\right)\right] - \exp\left(-\zeta T_{\text{slot}}\right)}\right\} \\ &= \frac{1}{2} + \frac{1}{2}\text{erf}\left\{\frac{\ln\left\{\frac{\zeta T_{\text{burst}} x_{\text{ISI}}}{\exp[-\zeta(T_{\text{slot}}-T_{\text{burst}})]-\exp(-\zeta T_{\text{slot}})}\right\} - \mu_\rho}{\sqrt{2}\sigma_\rho}\right\}, \end{aligned} \tag{32}$$

by noting that $T_{\text{slot}} > T_{\text{burst}}$ and ρ follows a lognormal distribution as expressed in (3). The term $\text{erf}\{\cdot\}$ denotes the error function and the subscript ISI indicates that the threshold is related to: inter-symbol interference.

Subsequently, provided with another threshold x_{NFD} and following (32), the duration when the contrast agent concentration is above x_{NFD} at each symbol time is expressed as

$$\begin{aligned} \Delta t &= t_u\left(x_{\text{NFD}}\right) - t_l\left(x_{\text{NFD}}\right) \\ &= -\frac{1}{\zeta}\ln\left\{\frac{\zeta T_{\text{burst}} x_{\text{NFD}}}{\rho\left[\exp\left(\zeta T_{\text{burst}}\right) - 1\right]}\right\} \\ &\quad - \left[-\frac{1}{\zeta}\ln\left(1 - \frac{\zeta T_{\text{burst}} x_{\text{NFD}}}{\rho}\right)\right] \\ &= \frac{1}{\zeta}\ln\left\{\frac{\left[\exp\left(\zeta T_{\text{burst}}\right) - 1\right]\left(\rho - \zeta T_{\text{burst}} x_{\text{NFD}}\right)}{\zeta T_{\text{burst}} x_{\text{NFD}}}\right\}, \end{aligned} \tag{33}$$

where t_u and t_l are the intersections of the straight line $x_{\text{R}}(t) = x_{\text{NFD}}$ and the curve drawn from (31). The subscript NFD indicates that the threshold is related to non-fade duration. By applying (33) and (3), the probability that Δt is no less than a threshold Δt_{NFD} is given by:

$$\begin{aligned} P_{\text{NFD}} &= \Pr\left\{\Delta t \ge \Delta t_{\text{NFD}}\right\} \\ &= \Pr\left\{\rho \ge \frac{\zeta T_{\text{burst}} x_{\text{NFD}} \exp\left(\zeta \Delta t_{\text{NFD}}\right)}{\exp\left(\zeta T_{\text{burst}}\right) - 1} + \zeta T_{\text{burst}} x_{\text{NFD}}\right\} \\ &= \frac{1}{2} \\ &\quad - \frac{1}{2}\text{erf}\left\{\frac{\ln\left\{\frac{\zeta T_{\text{burst}} x_{\text{NFD}} \exp(\zeta \Delta t_{\text{NFD}})}{\exp(\zeta T_{\text{burst}})-1} + \zeta T_{\text{burst}} x_{\text{NFD}}\right\} - \mu_\rho}{\sqrt{2}\sigma_\rho}\right\}. \end{aligned} \tag{34}$$

A. Maximization of P_{ISI} and P_{NFD}

The inter-symbol interference and non-fade duration criteria for the touchable communication waveform design aim at finding the values of T_{burst} such that P_{ISI} and P_{NFD} in (32) and (34) are maximized.

In the situation that there is a tradeoff between P_{ISI} and P_{NFD}, the Pareto efficiency can be applied. It is a concept in multi-criteria optimization enabling all tradeoffs among the best combinations of multiple criteria to be evaluated. The objective here is to maximize P_{ISI} and P_{NFD} simultaneously, and the Pareto frontier is defined as the set of choices of $(P_{\mathrm{ISI}}, P_{\mathrm{NFD}})$ whereby any improvement with respect to P_{ISI} comes at the expense of P_{NFD}. Each point along that frontier represents a unique parameterization of the transmitted signal $x_{\mathrm{T}}(t)$ in terms of its pulse duration T_{burst}, so the associated Pareto optimality identifies multiple Pareto solutions of $(P_{\mathrm{ISI}}, P_{\mathrm{NFD}})$. Through this procedure one is able to investigate differences among the multiple solutions that are able to optimize varying combinations of the two assessment criteria.

The aforementioned Pareto efficiency strategy for waveform design can be formally expressed as follows. Consider the system with function $\mathcal{F} : \mathbb{R}_{[0,T_{\mathrm{slot}}]} \rightarrow \mathbb{R}^2_{[0,1]}$, where $\mathbb{X}$ is a compact set of feasible decisions of T_{burst} in the space $\mathbb{R}_{[0,T_{\mathrm{slot}}]} = \{x \in \mathbb{R} | 0 \leq x \leq T_{\mathrm{slot}}\}$ and $\mathbb{Y}$ is the feasible set of criterion vectors $(P_{\mathrm{ISI}}, P_{\mathrm{NFD}})$ in $\mathbb{R}^2_{[0,1]} = \{y \in \mathbb{R} | 0 \leq y \leq 1\} \times \{y \in \mathbb{R} | 0 \leq y \leq 1\}$. Larger criteria values are preferred to smaller ones. A point $y'' \in \mathbb{R}^2_{[0,1]}$ is preferred to (strictly dominates) another point $y' \in \mathbb{R}^2_{[0,1]}$, written as $y'' \succ y'$. The Pareto frontier is thus written as:

$$\left\{y' \in \mathbb{Y} : \left\{y'' \in \mathbb{Y} : y'' \succ y', y'' \neq y'\right\} = \varnothing\right\}. \tag{35}$$

The Pareto optimum criterion aims at finding the set of T_{burst} such that the Pareto frontier is achieved.

B. Minimization of BER

As described in Section II-A, bits '1' and '0' are represented by a burst of drug molecules within a time slot and the absence of molecules, respectively. It is thus assumed that the event of an erroneous bit occurs under the following two conditions. When a bit '0' is transmitted, the receiver (tumor) detects the bit to be '1' if the duration when the drug concentration is above x_{NFD} is no less than Δt_{NFD} within the symbol time. On the other hand, a bit '1' is incorrectly detected as '0' if this duration is less than Δt_{NFD}.

Subsequently, by ignoring counting errors at the receiver (i.e., all drug molecules delivered by nanorobots to the tumor will be bound to cancer cell receptors), the BER can be derived as

$$\begin{aligned}
&P_e \\
&= \Pr\left\{\hat{b}_j = 1 \middle| b_j = 0\right\} \Pr\left\{b_j = 0\right\} \\
&+ \Pr\left\{\hat{b}_j = 0 \middle| b_j = 1\right\} \Pr\left\{b_j = 1\right\} \\
&\approx \Pr\left\{\hat{b}_j = 1 \middle| b_j = 0; b_{j-1} = 1\right\} \Pr\left\{b_j = 0\right\} \Pr\left\{b_{j-1} = 1\right\} \\
&+ \Pr\left\{\hat{b}_j = 0 \middle| b_j = 1; b_{j-1} = 0\right\} \Pr\left\{b_j = 1\right\} \Pr\left\{b_{j-1} = 0\right\} \\
&+ \Pr\left\{\hat{b}_j = 0 \middle| b_j = 1; b_{j-1} = 1\right\} \Pr\left\{b_j = 1\right\} \Pr\left\{b_{j-1} = 1\right\},
\end{aligned} \tag{36}$$

where b_j denotes the j^{th} bit and $\Pr\{\cdot|\cdot\}$ is the conditional probability. Eq. (36) assumes that only the $(j-1)^{\mathrm{th}}$ bit has impact on the detection of the j^{th} bit, because the concentration-time profiles for earlier bits decay quickly with time.

The event $\left\{\hat{b}_j = 1 \middle| b_j = 0; b_{j-1} = 1\right\}$ occurs when the inter-symbol interference due to the $(j-1)^{\mathrm{th}}$ bit is above a certain value, resulting in the duration when the drug concentration is above x_{NFD} at the j^{th} bit is no less than Δt_{NFD}, i.e.,

$$\begin{aligned}
&t_u\left(x_{\mathrm{NFD}}\right) - T_{\mathrm{slot}} \geq \Delta t_{\mathrm{NFD}} \\
&\Rightarrow -\frac{1}{\zeta} \ln\left\{\frac{\zeta T_{\mathrm{burst}} x_{\mathrm{NFD}}}{\rho\left[\exp\left(\zeta T_{\mathrm{burst}}\right) - 1\right]}\right\} - T_{\mathrm{slot}} \geq \Delta t_{\mathrm{NFD}} \\
&\Rightarrow \rho \geq \frac{\zeta T_{\mathrm{burst}} x_{\mathrm{NFD}}}{\left[\exp\left(\zeta T_{\mathrm{burst}}\right) - 1\right] \exp\left[-\zeta\left(T_{\mathrm{slot}} + \Delta t_{\mathrm{NFD}}\right)\right]}.
\end{aligned} \tag{37}$$

Consequently, the following conditional probability is given by

$$\begin{aligned}
&\Pr\left\{\hat{b}_j = 1 \middle| b_j = 0; b_{j-1} = 1\right\} \\
&= \Pr\left\{\rho \geq \frac{\zeta T_{\mathrm{burst}} x_{\mathrm{NFD}}}{\left[\exp\left(\zeta T_{\mathrm{burst}}\right) - 1\right] \exp\left[-\zeta\left(T_{\mathrm{slot}} + \Delta t_{\mathrm{NFD}}\right)\right]}\right\} \\
&= \frac{1}{2} - \frac{1}{2}\mathrm{erf}\left\{\frac{\ln\left\{\frac{\zeta T_{\mathrm{burst}} x_{\mathrm{NFD}}}{\left[\exp\left(\zeta T_{\mathrm{burst}}\right) - 1\right] \exp\left[-\zeta\left(T_{\mathrm{slot}} + \Delta t_{\mathrm{NFD}}\right)\right]}\right\} - \mu_\rho}{\sqrt{2}\sigma_\rho}\right\}.
\end{aligned} \tag{38}$$

Furthermore, the event $\left\{\hat{b}_j = 0 \middle| b_j = 1; b_{j-1} = 0\right\}$ is complementary to the non-fade event in (34) because there is no inter-symbol interference from the $(j-1)^{\mathrm{th}}$ bit. Thus,

$$\Pr\left\{\hat{b}_j = 0 \middle| b_j = 1; b_{j-1} = 0\right\} = 1 - P_{\mathrm{NFD}}. \tag{39}$$

Next, the event $\left\{\hat{b}_j = 0 \middle| b_j = 1; b_{j-1} = 1\right\}$ occurs when the summation of the residual drug molecules from the $(j-1)^{\mathrm{th}}$ bit and the drug entering the tumor for the j^{th} bit is too low to achieve correct detection of bit 1. The two time instants when the drug concentration is equal to x_{NFD} are first calculated by applying (31) and assuming that the propagation channels for two consecutive bits are fully correlated. For $T_{\mathrm{slot}} \leq t_l \leq T_{\mathrm{slot}} + T_{\mathrm{burst}}$, the following relationship is satisfied:

$$\begin{aligned}
&\frac{\rho\left\{\exp\left[-\zeta\left(t_l - T_{\mathrm{burst}}\right)\right] - \exp\left(-\zeta t_l\right)\right\}}{\zeta T_{\mathrm{burst}}} \\
&+ \frac{\rho\left[1 - \exp\left[-\zeta\left(t_l - T_{\mathrm{burst}}\right)\right]\right]}{\zeta T_{\mathrm{burst}}} = x_{\mathrm{NFD}},
\end{aligned} \tag{40}$$

resulting in

$$t_l = -\frac{1}{\zeta}\ln\left(1 - \frac{\zeta T_{\text{burst}} x_{\text{NFD}}}{\rho}\right). \tag{41}$$

On the other hand, for $T_{\text{slot}} + T_{\text{burst}} < t_u \leq 2T_{\text{slot}}$, we have

$$x_{\text{NFD}} = \frac{\rho\left\{\exp\left[-\zeta\left(t_u - T_{\text{burst}}\right)\right] - \exp\left(-\zeta t_u\right)\right\}}{\zeta T_{\text{burst}}} + \frac{\rho\left\{\exp\left[-\zeta\left(t_u - 2T_{\text{burst}}\right)\right] - \exp\left[-\zeta\left(t_u - T_{\text{burst}}\right)\right]\right\}}{\zeta T_{\text{burst}}}, \tag{42}$$

giving rise to

$$t_u = -\frac{1}{\zeta}\ln\left\{\frac{\zeta T_{\text{burst}} x_{\text{NFD}}}{\rho\left[\exp\left(2\zeta T_{\text{burst}}\right) - 1\right]}\right\}. \tag{43}$$

By applying the similar approach to (33) and (34), the following conditional probability is obtained:

$$\begin{aligned}
&\Pr\left\{\hat{b}_j = 0 \middle| b_j = 1; b_{j-1} = 1\right\} \\
&= \Pr\left\{\rho \leq \frac{\zeta T_{\text{burst}} x_{\text{NFD}} \exp\left(\zeta \Delta t_{\text{NFD}}\right)}{\exp\left(2\zeta T_{\text{burst}}\right) - 1} + \zeta T_{\text{burst}} x_{\text{NFD}}\right\} \\
&= \frac{1}{2} \\
&+ \frac{1}{2}\text{erf}\left\{\frac{\ln\left\{\frac{\zeta T_{\text{burst}} x_{\text{NFD}} \exp(\zeta \Delta t_{\text{NFD}})}{\exp(2\zeta T_{\text{burst}}) - 1} + \zeta T_{\text{burst}} x_{\text{NFD}}\right\} - \mu_\rho}{\sqrt{2}\sigma_\rho}\right\}
\end{aligned} \tag{44}$$

Substituting (38), (39), and (44) into (36) yields the closed-form expression of BER.

Finally, the BER criterion for the touchable communication waveform design aims at finding the optimal value of T_{burst} such that the BER in (36) is minimized.

Because the contrast agent concentration is proportional to the volume fraction and only the latter is estimated through the CMI system, the volume fraction will be used during the waveform design process.

V. Numerical Results and Analysis

A. System Settings for Simulation Study

A study case of CMI for optimal targeted therapies is presented in this section by applying the proposed communication waveform design strategies. The CMI of breast cancer is investigated as illustrated in Fig. 2. A single 1 cm diameter cancerous mass is placed in the breast with multiple tissue inhomogeneities. The dielectric properties of healthy breast tissues are governed by (4), where the "fat-medium" category in [23] is considered with the following model parameters: $F_1 = 3.140$, $F_2 = 1.708$, $F_3 = 14.65$ ps, $F_4 = 0.061$, and $F_5 = 0.036$ S/m. The dielectric values of tumor tissue are assumed to be fivefold those of healthy tissue across the whole band of interest [15], [24]. To emulate an uptake of contrast agent nanoparticles in malignant tissue, the complex permittivity of the inclusion vary with the volume fraction of drug molecules by following the mixture formula in (5). The contrast agent nanoparticles are assumed to have exceptionally high microwave-frequency dielectric properties such as the functionalizing CVD-synthesized carbon nanotubes *via* sonication in nitric and sulfuric acid investigated in [14]. The real and imaginary parts of the complex permittivity of the agent are assumed to be 200 and 100, respectively, over the band of interest [30]. The numerical phantom includes a skin layer with relative permittivity 36.0 and conductivity 4.0 S/m [26]. The thickness of the skin layer is 0.2 cm.

It is further assumed that antennas are immersed in a coupling medium with dielectric property matching the breast permittivity over the entire frequency band [26], which can be achieved by using various tissue-mimicking materials. The imaging system is comprised of an array of 41 elements located at 2 cm $\sim$ 42 cm from the tumor in an interval of 1 cm. Each antenna is driven with a modulated Gaussian monocycle with the modulation frequency 1 GHz and pulse width 120 ps [15], [26]. The reflected waveform is recorded at the same antenna (monostatic configuration). The backscatter signals received at the antennas are computed by applying (9). The accumulation of drug molecules in the tumor follows the input-output relationship in (2) and the corresponding impulse response in terms of volume fraction is given by (23). It is supposed that the mean and standard deviation of the natural logarithm of path loss from the injection site to the tumor are $\ln 0.2$ and 0.2, respectively. We consider three different elimination rates: $\zeta = 1.3$ day^{-1}, 1.5 day^{-1}, and 1.7 day^{-1} [18]. The difference between the postcontrast and precontrast signals is then computed for various concentrations of nanoparticles. This clean differential waveform is first corrupted by a multiplicative complex Gaussian vector process representing measurement uncertainties. Subsequently, an additive white Gaussian noise vector is added to the artifact-corrupted differential signal. The algorithm presented in Section III is then applied to estimate the normalized SNR at each antenna and the time-varying volume fraction of drug molecules.

The final step is to determine the desirable values of T_{burst} for optimal targeted therapies by employing the inter-symbol interference, non-fade duration, and BER waveform design criteria in Section IV.

B. Numerical Results

The dielectric constant and conductivity of tumor mixed with various volume fractions of drug molecules are shown in Fig. 3. Both the dielectric properties increase with volume fraction. On the other hand, the dielectric constant decreases and the conductivity increases as the frequency increases. Fig. 4 depicts the relationships between the normalized SNR $\bar{\eta}_{z^*(t)}$ and the normalized volume fraction $V_{\text{agent}}(t)/V_{\text{agent}}(0)$ by applying the exact formulation in Section II-C and the approximation in (22) with $\kappa = 1.75$, respectively. The approximation matches well the exact solution throughout the entire range of $V_{\text{agent}}(t)/V_{\text{agent}}(0)$.

Fig. 5 plots the relationships between the estimated rank of $\Delta\boldsymbol{\Psi}_z$ in (20) and the SNR of differential signal by utilizing the Akaike information criterion and the maximum description length, respectively. As can be seen from this figure, the rank decreases as SNR reduces and the threshold SNRs can be obtained when the rank has just turned to zero, which verifies

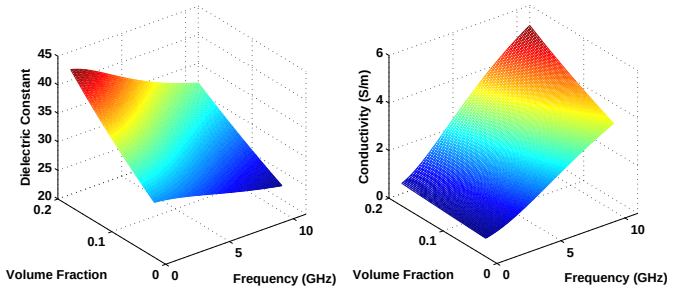

Fig. 3. (a) Dielectric constant and (b) conductivity of tumor mixed with various volume fractions of drug molecules.

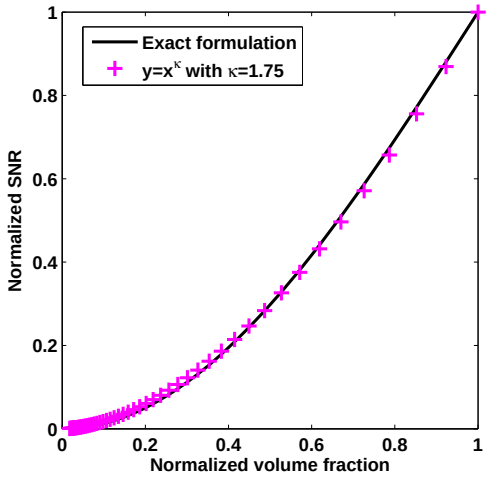

Fig. 4. Relationships between the normalized SNR and the normalized volume fraction by applying the exact formulation in Section II-C and the approximation in (22), respectively.

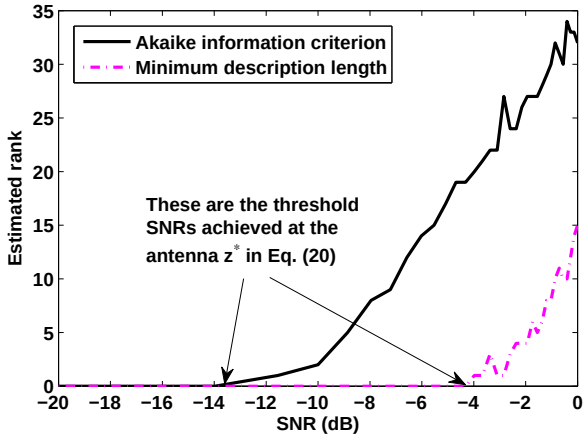

Fig. 5. Relationships between the estimated rank of $\Delta\Psi_z$ in (20) and the SNR of the differential signal for two information-theoretic criteria.

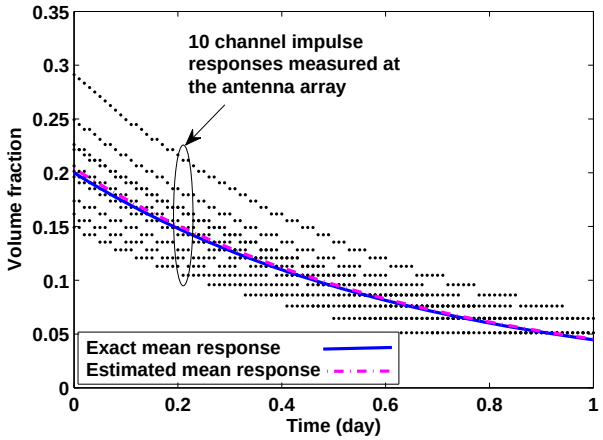

Fig. 6. 10 pilot channel impulse responses measured at the antenna array. Also shown are the exact mean response with $\ln \mu_V = \ln 0.2$ and $\zeta = 1.5$ and the estimated mean response with $\ln \hat{\mu}_V = \ln 0.204$ and $\hat{\zeta} = 1.5035$. The estimated standard deviation is $\hat{\sigma}_V = 0.1924$, which is very close to the exact value of $\sigma_V = 0.2$.

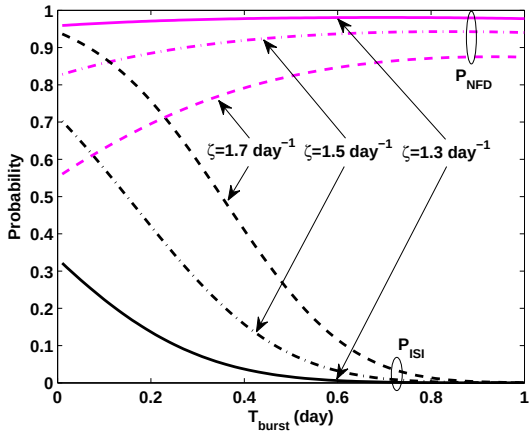

Fig. 7. Relationships between P_{ISI}, P_{NFD}, and T_{burst} for various elimination rates.

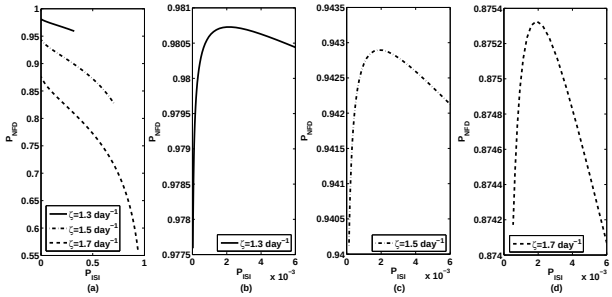

Fig. 8. (a) Pareto frontiers of $(P_{\mathrm{ISI}}, P_{\mathrm{NFD}})$ for various elimination rates, and the zoomed-in plots of (a) for (b) $\zeta = 1.3$ day^{-1}, (c) $\zeta = 1.5$ day^{-1}, and (d) $\zeta = 1.7$ day^{-1}.

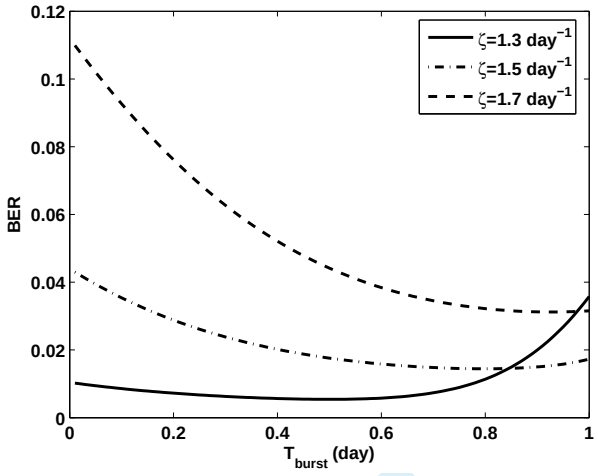

Fig. 9. Relationships between BER and $T_{\rm burst}$ for various elimination rates.

the effectiveness of the algorithm presented in (20) and (21). It is worth noting that the Akaike information criterion is more sensitive than the maximum description length at the low SNR regime.

Fig. 6 shows 10 independent pilot channel responses measured by the CMI system. Due to the discrete structure of the antenna array, the impulse responses are discretized as well. Also shown are the exact mean response with $\mu_V = \ln 0.2$ and $\zeta = 1.5$ and the estimated mean response with $\hat{\mu}_V = \ln 0.204$ and $\hat{\zeta} = 1.5035$. As demonstrated in Fig. 6, the exact model parameters of the lognormal distribution and exponential clearance agree well with the estimated values. Furthermore, the estimated standard deviation is $\hat{\sigma}_V = 0.1924$, which is very close to the exact value of $\sigma_V = 0.2$.

The relationships between $P_{\rm ISI}$, $P_{\rm NFD}$, and $T_{\rm burst}$ for various values of drug clearance rate ζ are depicted in Fig. 7. As shown in this figure, as ζ decreases, $P_{\rm ISI}$ decreases leading to more severe inter-symbol interference. On the contrary, $P_{\rm NFD}$ increases with reduced ζ, indicating longer duration when the drug concentration is above a threshold level during each symbol time. In general, $P_{\rm ISI}$ decreases whereas $P_{\rm NFD}$ increases as $T_{\rm burst}$ increases.

The Pareto frontiers of $(P_{\rm ISI}, P_{\rm NFD})$ for various elimination rates are drawn in Fig. 8(a), which agree with the trend observed in Fig. 7. The zoomed-in versions of Fig. 8(a) for $\zeta = 1.3$ day^{-1}, $\zeta = 1.5$ day^{-1}, and $\zeta = 1.7$ day^{-1} are shown in Fig. 8(b)-(c), respectively. Noteworthily, in the regime of small $P_{\rm ISI}$ (less than ~ 0.002), $P_{\rm NFD}$ increases with $P_{\rm ISI}$ and the Pareto optimality does not exist. In this case, there is no tradeoff between these two probabilities and a single $T_{\rm burst}$ can be found to maximize both the probabilities simultaneously.

Finally, Fig. 9 demonstrates the relationships between BER and $T_{\rm burst}$ for various values of elimination rate ζ. It can be seen that overall, a larger ζ results in a larger BER, though there are some crossovers when $T_{\rm burst}$ approaches 1 day. For all the clearance rates, the optimum $T_{\rm burst}$ that result in minimum BERs can be acquired. Moreover, the optimum $T_{\rm burst}$ increases with ζ.

VI. Conclusion

A novel model of CMI-assisted optimal TDD from the perspective of touchable communication channel estimation and waveform design has been proposed. The CMI technique has been employed as a pretherapeutic evaluation technique to determine the pharmacokinetic model, where an information-theoretic-criteria-based signal processing algorithm was applied to estimate drug accumulation in tumor. This step is analogous to the estimation of channel impulse response in the classical communication systems. Three TDD optimization strategies have been introduced. These strategies are based on minimization of residual drug molecules at the end of each therapeutic session (i.e., inter-symbol interference), maximization of duration that the drug intensity is above a prespecified threshold during each therapeutic session (i.e., non-fade duration), and minimization of average rate that a therapeutic operation is not received correctly at tumor (i.e., BER). Finally, comprehensive numerical examples have been presented to demonstrate the key processes and properties of the proposed analytical framework. The current work may provide useful insight on realistic and clinically relevant design and implementation of touchable communication systems for targeted therapies.

References

[1] O. M. Koo, I. Rubinstein, and H. Onyuksel, "Role of nanotechnology in targeted drug delivery and imaging: a concise review," *Nanomed.*, vol. 1, no. 3, pp. 193–212, Sep. 2005.

[2] O. Felfoul, M. Mohammadi, S. Taherkhani, and et al., "Magneto-aerotactic bacteria deliver drug-containing nanoliposomes to tumour hypoxic regions," *Nature Nanotechnology*, pp. 1–7, 2016, Advance Online Publication, DOI: 10.1038/NNANO.2016.137.

[3] L. Mellal, D. Folio, K. Belharet, and A. Ferreira, "Modeling of optimal targeted therapies using drug-loaded magnetic nanoparticles for the liver cancer," *IEEE Trans. Nanobiosci.*, vol. 15, no. 3, pp. 265–274, Apr. 2016.

[4] Y. Chahibi, M. Pierobon, S. O. Song, and I. F. Akyildiz, "A molecular communication system model for particulate drug delivery systems," *IEEE Trans. Biomed. Eng.*, vol. 60, no. 12, pp. 3468–3483, Dec. 2013.

[5] Y. Chahibi and I. F. Akyildiz, "Molecular communication noise and capacity analysis for particulate drug delivery systems," *IEEE Trans. Commun.*, vol. 62, no. 11, pp. 3891–3903, Nov. 2014.

[6] Y. Chahibi, I. F. Akyildiz, S. Balasubramaniam, and Y. Koucheryavy, "Molecular communication modeling of antibody-mediated drug delivery systems," *IEEE Trans. Biomed. Eng.*, vol. 62, no. 7, pp. 1683–1695, July 2015.

[7] Y. Chahibi, M. Pierobon, and I. F. Akyildiz, "Pharmacokinetic modeling and biodistribution estimation through the molecular communication paradigm," *IEEE Trans. Biomed. Eng.*, vol. 62, no. 10, pp. 2410–2420, Oct. 2015.

[8] Y. Chen, P. Kosmas, P. S. Anwar, and L. Huang, "A touch-communication framework for drug delivery based on a transient microbot system," *IEEE Trans. NanoBiosci.*, vol. 14, no. 4, pp. 397–408, June 2015.

[9] M. Femminella, G. Reali, and A. V. Vasilakos, "A molecular communications model for drug delivery," *IEEE Trans. Nanobiosci.*, vol. 14, no. 8, pp. 935–945, Dec. 2015.

[10] U. A. K. Chude-Okonkwo, R. Malekian, and B. T. Sunil Maharaj, "Molecular communication model for targeted drug delivery in multiple disease sites with diversely expressed enzymes," *IEEE Trans. Nanobiosci.*, vol. 15, no. 3, pp. 230–245, Apr. 2016.

[11] Y. Chen, T. Nakano, P. Kosmas, C. Yuen, A. V. Vasilakos, and M. Asvial, "Green touchable nanorobotic sensor networks," *IEEE Commun. Mag.*, pp. 136–142, Nov. 2016.

[12] T. Nakano, S. Kobayashi, T. Suda, Y. Okaie, Y. Hiraoka, and T. Haraguchi, "Externally controllable molecular communication," *IEEE J. Sel. Areas Commun.*, vol. 32, no. 12, pp. 2417–2431, Dec. 2014.

[13] A. Mashal, B. Sitharaman, X. Li, P. K. Avti, A. V. Sahakian, J. H. Booske, and S. C. Hagness, "Toward carbon-nanotube-based theranostic agents for microwave detection and treatment of breast cancer: Enhanced dielectric and heating response of tissue-mimicking materials," *IEEE Trans. Biomed. Eng.*, vol. 57, pp. 1831–1834, Aug. 2010.

[14] S. X. Xie, F. Gao, S. C. Patel, J. H. Booske, S. C. Hagness, and B. Sitharaman, "Clinically relevant CNT dispersions with exceptionally high dielectric properties for microwave theranostic applications," *IEEE Trans. Biomed. Eng.*, vol. 61, no. 11, pp. 2718–2723, 2014.

[15] Y. Chen and P. Kosmas, "Detection and localization of tissue malignancy using contrast-enhanced microwave imaging: Exploring information theoretic criteria," *IEEE Trans. Biomed. Eng.*, vol. 59, pp. 766–776, Mar. 2012.

[16] A. Ergun, K. Camphausen, and L. W. Wein, "Optimal scheduling of radiotherapy and angiogenic inhibitors," *Bulletin of Mathematical Biology*, vol. 65, no. 3, pp. 407–424, 2003.

[17] L. G. de Pillis, W. Gu, K. R. Fister, T. A. Head, K. Maples, A. Murugan, T. Neal, and K. Yoshida, "Chemotherapy for tumors: An analysis of the dynamics and a study of quadratic and linear optimal controls," *Mathematical Biosciences*, vol. 209, no. 1, pp. 292–315, 2007.

[18] P. Hahnfeldt, D. Panigrahy, J. Folkman, and L. Hlatky, "Tumor development under angiogenic signaling a dynamical theory of tumor growth, treatment response, and postvascular dormancy," *Cancer Research*, vol. 59, no. 19, pp. 4770–4775, 1999.

[19] Q. Zhou, P. Guo, G. D. Kruh, P. Vicini, X. Wang, and J. M. Gallo, "Predicting human tumor drug concentrations from a preclinical pharmacokinetic model of temozolomide brain disposition," *Cancer Therapy: Preclinical*, vol. 13, no. 14, pp. 4271–4279, 2007.

[20] Y. Chen, P. Kosmas, and S. Martel, "Microwave breast tumor detection and size estimation using contrast-agent-loaded magnetotactic bacteria," in *Proc. IEEE EMBC 2013*, Osaka, Japan, Jul. 2013.

[21] S. Semenov, N. Pham, and S. Egot-Lemaire, "Ferroelectric nanoparticles for contrast enhancement microwave tomography: Feasibility assessment for detection of lung cancer," in *Proc. World Congress on Medical Physics and Biomedical Engineering*, Munich, Germany, Sep. 2009.

[22] G. Bellizzi, O. M. Bucci, and I. Catapano, "Microwave cancer imaging exploiting magnetic nanoparticles as contrast agent," *IEEE Trans. Biomed. Eng.*, vol. 58, pp. 2528–2536, Sept. 2011.

[23] E. Zastrow, S. K. Davis, M. Lazebnik, F. Kelcz, B. D. Van Veen, and S. C. Hagness, "Development of anatomically realistic numerical breast phantoms with accurate dielectric properties for modeling microwave interactions with the human breast," *IEEE Trans. Biomed. Eng.*, vol. 55, pp. 2792–2800, Dec. 2008.

[24] M. Lazebnik, D. Popovic, L. McCartney, C. B.Watkins, M. J. Lindstrom, J. Harter, S. Sewall, T. Ogilvie, A. Magliocco, T. M. Breslin, W. Temple, D. Mew, J. H. Booske, M. Okoniewski, and S. C. Hagness, "A large-scale study of the ultrawideband microwave dielectric properties of normal, benign and malignant breast tissues obtained from cancer surgeries," *Phys. Med. Biol.*, vol. 52, pp. 6093–6115, 2007.

[25] O. Levy and D. Stroud, "Maxwell Garnett theory for mixtures of anisotropic inclusions: Application to conducting polymers," *Physical Review B*, vol. 56, no. 13, pp. 8035–8046, 1997.

[26] Y. Chen, E. Gunawan, K. S. Low, S.-C. Wang, Y. Kim, and C. B. Soh, "Pulse design for time reversal method as applied to ultrawideband microwave breast cancer detection: A two-dimensional analysis," *IEEE Trans. Antennas Propag.*, vol. 55, no. 1, pp. 194–204, 2007.

[27] W. D. Burside and K. W. Burgener, "High frequency scattering by thin lossless dielectric slab," *IEEE Trans. Antennas Propag.*, vol. AP-31, no. 1, pp. 104–110, 1983.

[28] E. W. Weisstein, "Least squares fitting - Exponential," *MathWorld - A Wolfram Web Resource*, http://mathworld.wolfram.com/LeastSquaresFittingExponential.html.

[29] S. M. Kay, *Fundamentals of Statistical Signal Processing: Estimation Theory*, Prentice-Hall, New Jersey, 1993.

[30] S. Bianco, *Carbon Nanotubes - From Research to Applications*, InTech, 2011.